Sun, ocean, climate and atmospheric 14CO2 : an evaluation of causal and spectral relationships

Minze Stuiver and Thomas F. Braziunas

The Holocene 1993 3: 289
DOI: 10.1177/095968369300300401

The Holocene, 3,4 (1993) pp. 289–305

Sun, ocean, climate and atmospheric $^{14}CO_2$: an evaluation of causal and spectral relationships

Minze Stuiver and Thomas F. Braziunas

(Department of Geological Sciences, Quaternary Research Center and Joint Institute for the Study of the Atmosphere and Ocean (JISAO), University of Washington, Seattle, Wa 98195, USA)

Received 1 March 1993; revised manuscript accepted 20 May 1993

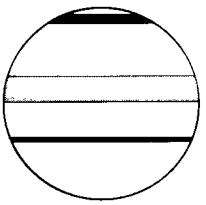

A
HOLOCENE
RESEARCH
PAPER

Abstract: Solar (heliomagnetic), geomagnetic and oceanic forcing all play a role in atmospheric $^{14}CO_2$ change. Here we assign the variance associated with certain periodicities in a single year (0–450 cal. BP) and a Holocene bidecadal (0–11 400 cal. BP) $^{14}CO_2$ record to specific forcing factors. In the single-year time series the variance in the 2–6-year periodicity range is attributable to El Niño–Southern Oscillation (ENSO) ocean perturbations. A 10–11-year component is partially tied to solar modulation of the cosmic ray flux, and multidecadal variability may relate to either solar modulation or instability of the North Atlantic thermohaline circulation. For the early Holocene bidecadal ^{14}C record we derive a 512-year atmospheric ^{14}C periodicity which relates to instabilities in North Atlantic thermohaline circulation. North Atlantic deep water formation increased near the start, instead of the termination, of the Younger Dryas interval. The ubiquitous 206-year ^{14}C cycle is assigned either to solar modulation, or to solar modulation modified by a climate (ocean) response. The latter modification is discussed as part of a hypothetical mechanism explaining postulated climate–^{14}C relationships in which a minor solar-induced Maunder Minimum climate change is amplified by salinity effects on North Atlantic thermohaline circulation.

Key words: radiocarbon, $^{14}CO_2$, solar forcing, periodicities, ENSO, thermohaline circulation, atmosphere–ocean interaction, Maunder Minimum, North Atlantic, Holocene.

Introduction

The palaeorecord of atmospheric $^{14}CO_2$ reveals substantial variability on timescales ranging from years to millenniums. World ocean salinity and circulation change influence climate as well as the $^{14}CO_2$ distribution between the atmosphere and the oceans. The influence on the atmospheric $^{14}CO_2$ record of ocean-related climatic change has to be weighed against ^{14}C production rate changes caused by geomagnetic and solar modulation of the cosmic ray flux. Here we try to unravel these contributions in 450- and 12 000-year-long records of, respectively, annual and bidecadal atmospheric $^{14}CO_2$ change.

The atmosphere, oceans and biosphere contain large amounts of exchangeable carbon. ^{14}C (half life $T = 5730$ years) is only a minor player in the carbon exchange between these reservoirs ($^{14}C/^{12}C$ ratio is about 10^{-12}), but it can readily be traced. The steady state total amount of ^{14}C in global exchangeable carbon approximates the average yearly ^{14}C production rate times the mean life of a ^{14}C atom ($T/\ln 2 = 8270$ years). The atmosphere and short-lived biosphere each contain about 100 years of ^{14}C production out of the 8270-year total, whereas the oceans contain most of the remainder. The ^{14}C residence time in the deep world ocean is of the order of 1000 years, and ^{14}C decay (1% per 83 years) lowers deep water specific ^{14}C activity (below 1000 m) by about 14% (based on GEOSECS measurements – Stuiver *et al.*, 1981) relative to the pre-AD 1850 surface (top 100 m) levels. Because the atmosphere exchanges $^{14}CO_2$ with the carbon species (bicarbonate, carbonate ions and dissolved CO_2) in the surface layer of the oceans, and because surface water ^{14}C levels depend on the rate of upwelling of older, deeper waters, the $^{14}CO_2$ content of the atmosphere depends not only on upper atmospheric ^{14}C production rates but also on the vagaries of a changeable ocean circulation (and air–sea gas exchange rate).

The dependence of cosmogenic ^{14}C production on solar wind properties is well established for the 11-year sunspot cycle (Lingenfelter, 1963; O'Brien, 1979). Longer-term production rate changes associated with periods of minimal sunspot activity also must contribute to atmospheric $^{14}CO_2$ variance (Stuiver and Quay, 1980). In a similar way, geomagnetic dipole change contributes to ^{14}C production rate variation (e.g., Mazaud *et al.*, 1991). The geomagnetic field and the magnetic properties of the solar wind each limit the influx of galactic cosmic rays so that increases in geomagnetic field

intensity and sunspot numbers cause lower ^{14}C production rates.

Solar and geomagnetic modulation of the cosmic ray flux, and ocean circulation/exchange rate variation, act in overlapping time domains. To complicate matters, they also need not always act independently. For instance, a solar change causing a ^{14}C production rate change could conceivably be related to a change in energy output (solar 'constant') and be accompanied by climatic change. This in turn could influence gas exchange rates (via wind speed) between the atmosphere and the mixed layer of the surface ocean, or cause salinity changes (via fresh water input) that influence thermohaline (upwelling) ocean circulation.

As a practical subdivision, we focus below on the 2–80-year periodicities in the single-year atmospheric $^{14}CO_2$ record and then continue with a discussion of the 80–2600-year periodicities in the much longer bidecadal record.

Annual and decadal $\Delta^{14}C$ change

Atmospheric $^{14}CO_2$ content is expressed as $\Delta^{14}C$, which is the relative deviation of the measured ^{14}C activity from the National Bureau Standards oxalic acid standard activity, after correction for isotope fractionation and radioactive decay related to age (Stuiver and Polach, 1977). The Figure 1 circles depict the mostly single-ring $\Delta^{14}C$ values derived from beta counting of CO_2 gas. The fine structure of the record is given in the lower curve (3-year moving average, with a 15‰ offset). The $\Delta^{14}C$ values and radiocarbon are given in Table 1. Four US Pacific northwest Douglas firs and one Noble fir were used. Missing or duplicate rings are usually absent in trees grown in this environment, and calendar ages were obtained simply from ring counting. A listing of the trees and the wood preparation (mostly cellulose) is given in Stuiver (1993). The AD 1510–1625 and AD 1820–1950 data, published previously (Stuiver, 1982; Stuiver and Quay, 1981), have been corrected for minor amounts of radon in the counting process (Stuiver and Becker, 1993). ^{14}C free carbon dioxide released by fossil fuel combustion is responsible for

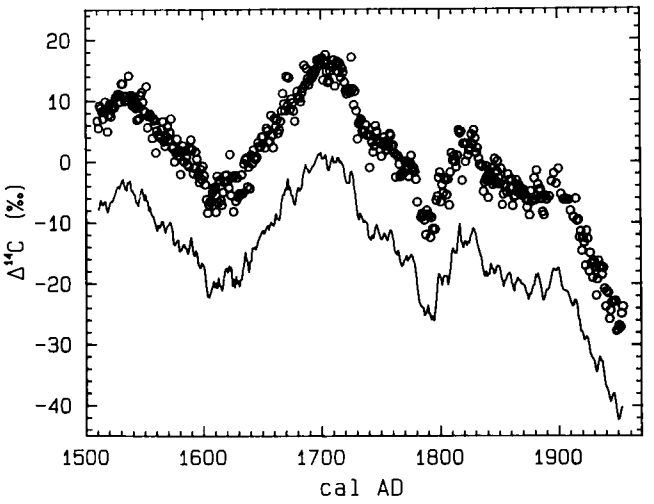

Figure 1 Atmospheric $\Delta^{14}C$ in per mil (circles), as derived from single rings of trees grown in the Pacific northwest. The fine structure of the data set is given in a 3-year moving average (lower curve, offset by 15‰). Exceptions to the single-year rule are 2-year data for AD 1890.5–1910.5 and 3-year data for AD 1913–1919. The calibrated (cal.) ages are based on ring counting. Approximate standard deviation in the measurements is 2‰.

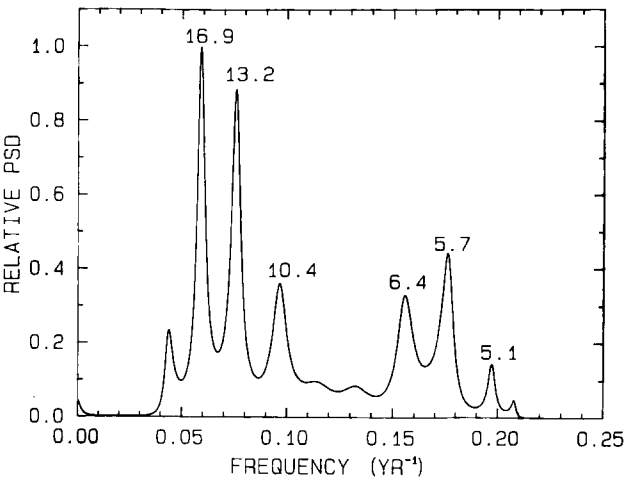

Figure 2 Relative power spectral density (PSD), normalized on the largest peak, obtained for the Figure 1 $\Delta^{14}C$ record from MEM (maximum entropy method) using the Burg algorithm with autoregressive (AR) order 43 or 13% of the length of the data record. The periods are given in years for each individual peak. The time interval analysed was AD 1510–1954; the spectrum was obtained after application of a 5–20-year split cosine band pass.

the pronounced twentieth-century $\Delta^{14}C$ reduction and has been discussed previously (Stuiver and Quay, 1981).

An obvious candidate for inducing decadal atmospheric $\Delta^{14}C$ change is solar modulation of the cosmic ray flux (sun mode $\Delta^{14}C$). Production rate changes (up to 25%) observed during several sunspot cycles suggest average atmospheric eleven-year $\Delta^{14}C$ variability in the range of 2 per mil (Stuiver and Quay, 1980). Such variability is close to the detection limit as the average standard deviation in the measurements is not much less than 2 per mil.

The data series contain, in addition to random noise, cyclic components that can be spectrally analysed. In the following discussion we consider first-order changes in spectral density but do not focus on quasi-stationary and random aspects.

For the 450-year annual record we confine our remarks to periodicities less than 80 years; the longer ones will be discussed with the 12 000-year bidecadal record. Periodicities in our MEM (maximum entropy method) power spectrum (Stuiver and Braziunas, 1989) for the AD 1510–1954 interval are at 56, 26, 17, 13, 10.4, 6.4, 5.7, 5.1, 3.5 and 2.7–2.1 years. The Figure 2 spectrum, obtained after application of a 5–20-year split cosine filter to the time series, depicts many of these frequencies. The periodicities in the 17–5.1-year range all have significance beyond the 2σ(σ = standard deviation) level in our Fourier analysis of the filtered signal. The 2.1–2.7-year periodicities are significant in the original time series as well, but these are not shown here due to the use of the filter.

Solar influences on ^{14}C production rate (11-year sunspot cycle) must relate to the 10.4-year periodicity, and perhaps to some of the longer ones, but the diverse composition of the spectrum suggests other contributing factors as well. Observation of the sun during the AD 1650–1715 (Maunder Minimum) interval indicates relatively minor sunspot activity (Eddy, 1976). The appearance of a quiet interval in the observations has supported the idea that extended intervals of low sunspot activity may occur.

To demonstrate the 11-year modulation we filtered the Figure 1 $\Delta^{14}C$ record with a 5–20-year period split cosine band pass. Filtering truncates the $\Delta^{14}C$ time series at each end (by 60 years in this case) because of the application of filter weights. Ordinarily our routine was first to extend the $\Delta^{14}C$ time series with zeros at each end, and subsequently to delete

Table 1

Cal AD	$\Delta^{14}C‰$	^{14}C age (BP)
1510.0	5.7±1.8	373.6±14.3
1511.0	5.5±1.7	382.5±13.3
1512.0	9.2±1.8	352.0±13.9
1513.0	8.8±1.8	354.1±14.3
1514.0	8.2±1.8	357.7±14.1
1515.0	7.0±1.6	366.4±13.1
1516.0	8.5±1.7	354.0±13.8
1517.0	9.9±1.8	341.9±14.4
1519.0	5.0±1.9	379.0±15.4
1520.0	7.7±1.8	356.2±14.1
1521.0	9.5±2.0	340.8±15.7
1522.0	7.4±2.0	356.3±15.8
1523.0	8.8±1.7	344.8±13.5
1524.0	9.2±1.8	340.3±14.2
1525.0	8.9±1.3	341.5±10.1
1526.0	10.6±1.8	327.4±14.2
1527.0	10.7±1.8	325.3±14.1
1528.0	11.1±1.6	321.0±13.0
1529.0	11.0±1.8	320.8±14.3
1530.0	9.8±1.8	329.4±14.3
1531.0	12.8±1.7	304.6±13.4
1532.0	12.8±1.3	303.8±10.2
1533.0	10.8±1.2	319.2± 9.7
1534.0	10.0±1.3	324.7±10.2
1535.0	10.8±1.2	317.2± 9.8
1536.0	10.1±1.3	321.1±10.2
1537.0	14.1±1.2	288.8± 9.6
1538.0	10.6±1.3	315.4±10.2
1539.0	10.9±1.3	312.1±10.3
1540.0	9.3±1.2	324.1± 9.9
1541.0	10.7±1.2	311.9± 9.4
1542.0	9.2±1.2	322.6± 9.8
1543.0	8.8±1.6	324.9±13.1
1544.0	6.9±1.7	339.5±13.9
1545.0	9.3±1.8	319.3±14.1
1546.0	7.1±1.8	335.7±14.5
1547.0	10.9±1.8	304.7±14.2
1548.0	11.4±1.8	299.6±14.2
1549.0	9.8±2.1	311.2±16.7
1550.0	8.4±1.1	321.9± 8.5
1551.0	8.2±2.0	322.5±15.6
1552.0	12.4±2.1	288.1±16.4
1553.0	5.6±1.8	340.5±14.4
1554.0	7.5±1.8	325.1±14.1
1555.0	7.9±1.7	320.6±13.3
1556.0	7.4±1.8	323.3±14.6
1557.0	3.9±1.8	350.7±14.4
1558.0	7.1±1.7	323.9±13.7
1559.0	6.8±1.8	325.5±14.4
1560.0	1.5±1.8	366.9±14.7
1561.0	5.1±1.8	337.1±14.4
1562.0	4.4±1.7	341.4±13.6
1563.0	4.4±1.8	340.8±14.4
1564.0	4.0±1.9	343.1±15.5
1565.0	5.4±1.9	330.8±15.2
1566.0	6.6±1.2	320.0± 9.8
1567.0	3.4±1.3	344.8±10.4
1568.0	2.6±1.8	350.4±14.6
1569.0	4.2±1.7	336.4±13.7
1570.0	5.8±1.8	322.7±14.5
1571.0	3.6±1.9	339.2±14.9
1572.0	4.9±1.8	328.2±14.0
1573.0	7.1±1.9	309.7±14.9
1574.0	2.3±1.8	346.6±14.4
1575.0	2.4±1.7	344.8±13.6
1576.0	0.1±1.8	362.9±14.4
1577.0	1.6±1.8	349.8±14.8
1578.0	3.8±1.7	331.0±13.6
1579.0	1.1±1.7	351.9±13.5
1580.0	1.9±1.7	344.0±14.0
1581.0	−2.0±1.8	374.7±14.3
1582.0	1.7±1.7	344.3±13.5
1583.0	2.7±1.7	334.9±13.4
1584.0	0.1±1.8	355.0±14.3
1585.0	1.9±1.8	339.6±14.6
1586.0	0.9±1.7	346.8±13.9
1587.0	−0.3±1.7	355.4±14.0
1588.0	−0.7±1.8	357.1±14.3
1589.0	2.3±1.7	332.0±13.5
1590.0	3.7±1.8	320.2±14.3
1591.0	2.1±1.7	332.0±13.9
1592.0	−1.8±2.0	362.6±15.9
1593.0	−0.9±1.7	354.1±13.4
1594.0	1.7±1.8	332.1±14.1
1595.0	0.6±1.7	340.4±13.8
1596.0	−2.1±1.7	361.2±14.1
1597.0	−3.3±1.8	369.4±14.6
1598.0	−1.1±1.7	351.1±14.0
1599.0	−2.8±1.8	363.3±14.3
1600.0	−0.6±1.2	345.1± 9.8
1601.0	−2.2±1.3	356.5±10.5
1602.0	−3.6±1.8	367.2±14.7
1603.0	−6.1±1.9	386.1±15.1
1604.0	−8.3±1.3	402.9±10.4
1605.0	−6.9±1.4	390.9±11.0
1606.0	−6.5±1.1	386.4± 9.0
1607.0	−6.4±2.0	384.6±16.0
1608.0	−4.9±1.4	371.5±11.5
1609.0	−4.4±1.6	367.1±12.6
1610.0	−4.0±1.8	363.0±14.6
1611.0	−8.1±1.3	395.0±10.5
1612.0	−2.2±1.8	346.4±14.4
1613.0	−6.6±1.7	380.6±14.1
1614.0	−2.9±1.8	350.1±14.7
1615.0	−6.2±1.3	375.3±10.2
1616.0	−7.0±1.7	381.0±13.9
1617.0	−4.9±1.8	363.0±14.7
1618.0	−3.2±1.7	348.2±14.0
1619.0	−2.1±1.8	338.5±14.2
1620.0	−2.0±1.3	336.9±10.2
1621.0	−3.0±1.8	343.9±14.4
1622.0	−4.1±1.3	352.1±10.3
1623.0	1.3±2.0	307.1±15.9
1624.0	−5.4±1.4	360.3±11.1
1625.0	−2.4±1.1	335.2± 9.0
1626.0	−8.1±1.8	379.8±14.6
1627.0	−2.1±1.8	331.1±14.8
1628.0	−6.3±1.8	364.0±14.5
1629.0	−2.5±1.2	331.9± 9.7
1630.0	−5.7±1.8	356.5±14.6
1631.0	−5.1±1.8	351.3±14.9
1632.0	−5.2±1.8	351.2±14.4
1633.0	−2.0±1.8	324.3±14.7
1634.0	−5.1±1.8	347.9±14.7
1635.0	−0.2±1.2	307.8± 9.9
1636.0	0.4±1.3	301.6±10.1
1637.0	0.7±2.2	298.3±17.4
1638.0	−4.0±1.7	335.4±13.7
1639.0	−0.8±1.1	308.1± 8.5
1640.0	−4.3±1.3	335.6±10.6
1641.0	1.2±2.2	290.7±17.3
1642.0	−0.2±1.8	300.9±14.1
1643.0	2.0±1.8	282.0±14.6
1644.0	0.8±1.0	291.2± 8.2
1645.0	0.5±1.7	292.1±13.8
1646.0	0.8±1.8	288.8±14.2
1647.0	3.2±1.9	268.5±15.5
1648.0	2.6±1.8	272.6±14.3
1649.0	2.5±1.3	272.2±10.0
1650.0	4.2±1.3	258.0±10.2
1651.0	4.2±1.9	256.9±15.1
1653.0	2.4±1.9	269.6±15.1
1654.0	5.6±1.3	243.0±10.3
1655.0	5.2±1.6	245.4±12.5
1656.0	3.3±1.6	259.5±13.1

Table 1 cont.

Cal AD	$\Delta^{14}C‰$	^{14}C age (BP)
1657.0	3.4±1.5	257.1±12.1
1658.0	7.7±1.9	222.2±15.1
1659.0	4.4±1.9	247.6±15.5
1660.0	2.4±1.3	262.5±10.1
1661.0	7.2±1.9	223.3±15.2
1662.0	5.8±1.8	233.3±14.5
1663.0	6.9±1.9	223.5±14.9
1664.0	4.7±1.1	240.0± 8.5
1665.0	5.3±1.4	234.4±11.3
1666.0	6.7±1.8	222.5±14.3
1667.0	8.4±1.9	207.9±14.7
1668.0	11.2±2.0	184.3±15.5
1669.0	9.5±1.9	196.8±14.8
1670.0	8.4±1.8	205.1±14.4
1671.0	14.0±1.3	159.3±10.5
1672.0	9.2±1.8	196.3±14.0
1673.0	13.8±1.3	159.0±10.1
1674.0	8.5±1.4	199.6±11.1
1675.0	10.3±1.7	184.9±13.8
1676.0	9.7±1.2	188.6± 9.8
1677.0	8.4±1.2	198.2± 9.4
1678.0	6.7±1.8	210.8±13.9
1680.0	11.6±1.7	170.1±13.3
1681.0	10.6±1.8	176.6±14.0
1682.0	10.4±1.9	176.9±15.1
1683.0	9.9±1.8	180.6±14.0
1684.0	11.4±1.8	167.5±14.4
1685.0	12.1±2.4	161.1±19.1
1686.0	15.8±0.9	128.3± 7.5
1687.0	12.7±1.1	152.6± 8.9
1688.0	15.3±1.3	130.5± 9.9
1689.0	13.7±1.3	142.7±10.6
1690.0	12.6±1.3	149.8±10.4
1691.0	13.4±1.0	143.7± 7.6
1692.0	14.5±1.0	133.9± 8.1
1693.0	13.8±1.0	138.5± 8.1
1694.0	14.9±0.9	128.9± 6.8
1695.0	14.5±0.8	131.2± 6.3
1696.0	15.1±1.0	124.9± 8.0
1697.0	16.7±1.1	111.6± 8.3
1698.0	15.8±1.1	117.6± 8.4
1699.0	16.7±1.1	109.7± 8.4
1700.0	16.1±0.9	113.2± 6.8
1701.0	17.0±1.0	103.3± 8.1
1702.0	13.4±0.8	132.0± 6.4
1703.0	16.4±0.9	108.3± 7.2
1704.0	17.6±0.9	96.4± 7.4
1705.0	14.8±1.3	117.7± 9.9
1706.0	13.0±1.3	131.1±10.2
1707.0	13.3±0.8	127.7± 6.7
1708.0	14.8±1.8	113.1±13.9
1709.0	15.8±1.3	105.9±10.4
1710.0	15.5±1.0	106.8± 7.8
1711.0	16.7±0.9	97.2± 6.8
1712.0	12.4±1.2	130.2± 9.8
1713.0	16.1±1.2	100.2± 9.9
1714.0	16.4±1.2	96.5± 9.6
1715.0	14.7±1.2	109.1± 9.7
1716.0	16.2±1.3	96.9±10.4
1717.0	13.8±1.0	113.4± 7.7
1718.0	15.4±0.8	101.0± 6.5
1719.0	14.7±1.0	104.8± 7.8
1720.0	13.0±1.0	116.6± 7.8
1721.0	11.6±1.2	127.6± 9.9
1722.0	11.1±1.2	131.0± 9.3
1723.0	12.0±1.3	122.9± 9.9
1724.0	11.5±1.0	126.3± 7.7
1725.0	11.3±1.1	126.1± 8.8
1726.0	17.1±1.5	77.5±11.5
1727.0	12.0±1.8	117.3±14.5
1728.0	9.3±1.8	137.4±14.5
1729.0	11.6±1.8	118.5±14.4
1730.0	8.4±1.8	143.1±14.5
1731.0	3.7±1.4	178.9±11.4
1732.0	6.3±1.4	157.6±11.5
1733.0	6.6±1.8	154.0±14.7
1734.0	7.0±2.3	150.0±18.3
1735.0	5.1±1.8	164.4±14.4
1736.0	5.1±2.0	163.0±15.8
1737.0	5.0±2.0	162.8±15.8
1738.0	6.0±1.7	153.7±13.8
1739.0	4.4±1.3	166.0±10.1
1740.0	4.4±1.7	164.6±13.8
1741.0	−0.9±1.3	206.8±10.2
1742.0	4.3±1.8	163.8±14.0
1743.0	3.3±1.1	171.1± 9.2
1744.0	1.6±1.7	183.6±13.9
1745.0	2.6±1.3	174.5±10.4
1746.0	5.9±1.2	147.1± 9.8
1747.0	5.0±1.7	153.4±13.9
1748.0	3.3±1.7	165.6±13.8
1750.0	3.2±1.2	165.0± 9.6
1751.0	0.9±1.3	182.3±10.5
1752.0	2.8±1.7	166.0±13.5
1753.0	4.0±1.1	155.3± 8.5
1754.0	3.3±1.8	160.2±14.0
1755.0	1.8±1.2	172.2± 9.8
1756.0	2.0±1.1	170.0± 8.6
1757.0	2.5±1.3	165.8±10.6
1758.0	4.6±1.0	148.3± 8.2
1759.0	4.3±1.3	149.1±10.0
1760.0	2.5±1.3	160.5±10.4
1761.0	2.7±1.2	157.9± 9.7
1762.0	1.4±1.7	167.6±13.8
1763.0	−2.5±1.7	198.2±13.3
1764.0	1.1±1.7	168.2±13.5
1765.0	0.9±1.7	168.8±13.8
1766.0	−0.4±1.7	178.1±13.7
1767.0	−2.5±1.7	193.8±13.6
1768.0	−2.0±1.7	189.0±13.9
1769.0	−1.8±1.7	186.4±13.8
1770.0	−1.8±1.7	185.9±13.5
1771.0	0.1±1.7	169.4±13.8
1772.0	−1.0±1.3	177.0±10.8
1773.0	−0.2±1.2	169.4± 9.7
1774.0	−2.4±1.7	186.8±13.4
1775.0	−0.1±1.7	167.1±13.5
1776.0	1.0±1.2	157.2± 9.6
1777.0	−1.4±1.3	175.6±10.3
1778.0	−0.9±1.7	170.9±13.5
1779.0	−1.6±1.7	175.2±13.6
1780.0	−2.9±1.2	184.6± 9.5
1781.0	−6.6±1.2	213.4± 9.6
1784.0	−9.1±1.7	234.6±14.1
1785.0	−8.5±1.4	228.9±11.6
1786.0	−8.9±2.3	231.0±19.0
1787.0	−9.5±1.7	235.3±13.8
1788.0	−11.9±1.8	254.0±14.9
1789.0	−7.9±1.8	220.5±14.3
1790.0	−8.6±1.7	225.1±14.0
1791.0	−8.8±1.8	225.6±14.6
1792.0	−12.4±1.8	253.8±14.7
1793.0	−9.1±1.7	226.2±14.2
1794.0	−11.0±1.7	240.6±14.2
1795.0	−11.0±2.0	239.2±15.9
1796.0	−11.1±1.8	239.0±14.2
1797.0	−6.3±1.7	199.7±13.6
1798.0	−5.7±1.2	193.5±10.1
1799.0	−2.6±1.7	167.9±14.1
1800.0	−1.7±1.7	159.8±14.1
1801.0	−6.6±1.2	198.1±10.1
1802.0	−3.8±1.3	174.7±10.2
1803.0	−5.1±1.7	184.3±14.0
1804.0	−2.8±1.7	164.6±13.5
1805.0	−2.9±1.7	164.5±13.6

Table 1 cont.

Cal AD	$\Delta^{14}C‰$	^{14}C age (BP)
1806.0	−5.4±1.8	183.8±14.1
1807.0	−2.9±1.3	162.3±10.6
1808.0	−7.1±1.8	195.5±14.2
1809.0	−1.8±1.8	151.1±14.4
1810.0	1.4±1.9	124.6±15.1
1811.0	0.2±2.0	133.6±15.8
1812.0	0.9±2.0	126.5±15.7
1813.0	0.0±1.2	133.3± 9.8
1814.0	−0.9±2.0	139.5±15.8
1815.0	1.0±1.8	123.2±14.2
1816.0	5.1±1.8	89.0±14.3
1817.0	4.6±1.9	92.1±15.5
1818.0	4.9±1.3	88.7±10.1
1819.0	−3.1±2.0	152.3±16.4
1820.0	2.9±1.0	102.8± 7.9
1821.0	3.0±1.0	101.3± 7.9
1822.0	0.0±1.2	124.6± 9.6
1823.0	3.0±1.7	99.7±13.4
1824.0	1.0±1.2	114.0± 9.6
1825.0	1.9±1.6	106.5±13.3
1826.0	2.2±1.6	102.5±13.0
1827.0	4.4±1.2	84.1± 9.4
1828.0	2.8±1.0	95.8± 7.8
1829.0	5.2±1.6	76.2±13.2
1830.0	3.8±1.6	86.0±12.9
1831.0	1.4±1.2	104.0±10.0
1832.0	2.2±1.4	96.8±10.9
1833.0	0.5±1.4	109.6±10.9
1834.0	−0.5±1.9	113.8±15.7
1835.0	−0.4±1.6	112.0±13.3
1836.0	−0.8±1.7	117.0±14.1
1837.0	−4.9±1.4	149.3±11.3
1838.0	−3.4±0.9	136.5± 7.5
1839.0	−3.0±2.6	131.6±20.7
1839.5	−0.8±1.6	113.5±13.2
1840.0	−2.5±2.5	127.3±20.3
1841.0	−5.9±1.7	154.2±14.0
1842.0	−1.7±1.4	118.6±11.0
1843.0	−2.3±1.0	122.5± 8.3
1844.0	−1.1±1.2	111.5± 9.7
1845.0	−3.8±2.5	132.7±20.3
1846.0	−2.8±2.5	123.4±20.1
1846.5	0.5±1.6	96.8±13.1
1847.0	−3.5±2.6	127.9±20.8
1848.0	−3.4±2.5	126.2±20.3
1848.5	−1.6±1.9	111.6±15.2
1849.0	0.1±2.5	97.7±20.0
1850.0	−2.7±2.5	119.0±20.3
1851.0	−3.7±2.5	126.2±20.3
1852.0	−1.2±2.5	104.8±20.0
1853.0	−7.1±2.5	151.2±20.5
1854.0	−5.4±2.6	136.4±20.7
1855.0	−4.0±1.6	124.6±12.8
1856.0	−4.0±1.2	123.6± 9.5
1857.0	−5.0±1.6	130.9±13.1
1858.0	−2.1±1.9	106.3±15.1
1859.0	−3.1±1.8	113.1±14.8
1860.0	−4.4±1.7	122.7±13.4
1861.0	−3.0±1.7	110.3±13.4
1862.0	−7.2±2.0	143.8±16.0
1863.0	−5.8±1.7	130.9±13.9
1864.0	−5.6±1.6	129.1±13.3
1865.0	−3.1±1.5	107.1±12.2
1866.0	−5.0±1.8	121.8±14.9
1867.0	−3.8±1.0	111.3± 8.3
1868.0	−4.4±1.3	115.4±10.5
1869.0	−5.0±1.3	119.1±10.1
1870.0	−5.6±1.3	122.5±10.6
1871.0	−4.6±1.4	114.2±11.3
1872.0	−5.3±1.1	118.5± 9.1
1873.0	−6.2±1.2	124.4± 9.9
1874.0	−7.5±1.8	134.4±14.3
1875.0	−6.4±1.1	124.4± 9.3
1876.0	−8.8±1.7	142.7±14.1
1877.0	−4.9±1.5	110.0±12.0
1878.0	−6.5±1.1	122.2± 9.2
1879.0	−6.4±1.5	120.8±12.3
1880.0	−2.7±1.6	90.1±12.9
1881.0	−6.3±1.6	117.6±13.1
1882.0	−1.5±1.2	77.8± 9.4
1883.0	−3.7±1.2	95.3± 9.8
1884.0	−4.7±1.7	101.8±13.8
1885.0	−4.5±1.2	99.7± 9.4
1886.0	−6.1±1.2	110.9± 9.4
1887.0	−8.2±1.1	127.6± 9.1
1888.0	−8.8±2.2	130.9±17.5
1889.0	−5.6±1.4	104.6±11.3
1890.5	−6.2±1.7	107.9±13.6
1892.5	−5.7±1.3	101.9±10.9
1894.5	−3.2±1.2	80.1± 9.8
1896.5	−1.9±1.7	67.5±13.8
1898.5	−3.6±1.9	79.3±15.6
1900.5	−1.2±2.0	57.7±16.1
1902.5	−5.3±1.5	89.0±11.9
1904.5	−6.2±1.7	94.1±13.6
1906.5	−6.1±1.2	91.5± 9.8
1908.5	−6.3±1.7	90.7±13.9
1910.5	−8.0±1.2	103.1± 9.6
1913.0	−9.1±0.8	109.3± 6.2
1915.0	−6.1±3.9	83.0±31.8
1916.0	−9.7±1.0	111.0± 7.9
1917.0	−9.5±1.2	108.6±10.1
1918.0	−12.4±1.2	131.2± 9.5
1919.0	−11.4±1.0	122.2± 8.2
1920.0	−14.6±1.8	147.2±14.6
1921.0	−12.4±1.8	128.4±14.7
1922.0	−13.2±1.8	134.3±14.9
1923.0	−17.1±1.6	164.4±13.1
1924.0	−11.3±1.7	116.7±13.8
1925.0	−12.6±1.6	126.3±13.1
1926.0	−18.0±1.6	168.9±13.1
1927.0	−15.0±2.1	143.5±17.3
1928.0	−16.7±1.7	156.7±14.3
1929.0	−19.0±1.2	174.7± 9.7
1930.0	−16.2±1.7	150.9±13.6
1931.0	−17.3±1.8	158.9±14.6
1932.0	−21.9±1.2	195.7±10.0
1933.0	−19.3±1.8	172.7±14.4
1934.0	−16.3±1.8	147.2±14.6
1935.0	−17.4±1.9	155.3±15.2
1936.0	−17.2±1.7	152.8±13.6
1937.0	−18.5±1.6	162.7±13.3
1938.0	−17.4±1.2	152.5± 9.9
1939.0	−20.8±1.8	179.5±15.1
1940.0	−23.7±2.0	202.6±16.3
1941.0	−21.3±1.9	181.4±15.5
1942.0	−21.5±1.2	182.2± 9.7
1943.0	−25.8±1.2	216.5±10.1
1944.0	−24.4±1.3	204.0±10.4
1945.0	−23.1±1.9	192.3±15.6
1947.0	−23.0±1.6	189.5±13.2
1948.0	−22.8±1.8	187.4±14.9
1949.0	−27.7±1.7	226.7±14.2
1950.0	−27.5±1.7	224.0±14.3
1951.0	−26.8±1.7	217.7±14.1
1952.0	−27.1±1.6	219.0±13.5
1953.0	−24.9±1.8	199.4±14.5
1954.0	−23.8±2.7	189.2±22.6

those years at the ends of each filtered record most influenced by the artificial extensions. A different approach was taken for the 5–20-year filtering, where the original record minus an 11-year moving average was used to extend each end (post-AD 1894 and pre-AD 1570). The removal of an 11-year average is justified by the observation that the filtered signal and the $\Delta^{14}C$ data from which an 11-year average is removed closely resemble each other.

For the full AD 1516–1948 filtered record we find the best match between inverted $\Delta^{14}C$ and sunspots when the $\Delta^{14}C$ calendar ages are reduced by 4 years. The $\Delta^{14}C$ signal was inverted in Figure 3 as lower sunspot activity induces less cosmic ray shielding, and thus higher ^{14}C production, within the earth's atmosphere.

Linear crosscorrelation between AD 1715–1948 sunspot numbers and Figures 3a and 3b $\Delta^{14}C$ data (here the $\Delta^{14}C$ calendar ages are already reduced by 4 years) yields a correlation coefficient $r = -0.39$. This r value corresponds to a 0.5% probability of the parameters not being correlated when autocorrelation (Quenouille, 1952) is taken into account. Accepting a 3-year lag instead leads to an r value of -0.32, with a 2.3% probability of not being correlated. Such a lag is close to the 2.5-year lag calculated for 11-year production rate forcing in our carbon reservoir model (Houtermans *et al.*, 1973; Braziunas, 1990).

Given the limited precision of the $\Delta^{14}C$ determinations, and the potential generation of atmospheric ^{14}C (creating inverse $\Delta^{14}C$ minima in Figure 3) by extremely energetic solar flares, a perfect agreement between $\Delta^{14}C$ and sunspot numbers cannot be expected. Centurial trends in inverted $\Delta^{14}C$ and sunspot numbers (and the Aa geomagnetic index) were shown to relate previously (Stuiver and Quay, 1980). Excellent agreement between inverted $\Delta^{14}C$ and sunspot numbers can be seen for several individual 11-year cycles (e.g., during the AD 1715–1760, 1845–1890 and 1905–1945 intervals) in Figures 3a and 3b. Although the low sunspot numbers associated with the Maunder Minimum suggest minimal 11-year modulation, the magnitude of the $\Delta^{14}C$ oscillations during the Maunder Minimum (AD 1650–1715) does not differ appreciably from those observed for the years preceding and following this interval (Figures 3a, 3b and 3c). When generating an artificial 11-year cycle (lower left of Figure 3b) that connects to the post-Maunder sunspot cyclicity, we also find the AD 1662 and 1673 inverted $\Delta^{14}C$ minima to be in phase with this artifical cycle. Although suggestive of the continuation of 11-year cycle modulation during the Maunder minimum, absolute proof cannot be given as only a limited portion of the $\Delta^{14}C$ variance (16% ($r = -0.39$) for the AD 1715–1948 interval) relates directly to sunspot numbers.

Figure 4, using the split cosine band pass filtering routine described above, depicts the $\Delta^{14}C$ oscillations near the 56-, 26-, 11- and 5-year periodicities. The respective ranges of periodicities allowed to pass unimpeded by these filters were: 40–65-, 25–35-, 5–20- and 2–5-year. The average 11-year cycle amplitude (each tick represents 1‰ on the vertical axis) indeed is larger than found for the surrounding cycles (1.4 per mil versus 1.0 per mil each for the 25- and 5-year periodicities) whereas 56-year cyclicity is strongest between AD 1700 and AD 1820.

The cosmogenic isotope ^{10}Be has been used to trace solar activity as well. The 11-year production rate variations for both ^{14}C and ^{10}Be are relatively large (in the range of 25%, peak to trough), but the ^{14}C signal recorded in tree-rings is strongly attenuated by the large atmospheric carbon reservoir, containing about 100 years of ^{14}C production. In our carbon reservoir model, the peak to trough change in atmospheric $\Delta^{14}C$ is 2.0 per mil on a global average basis for

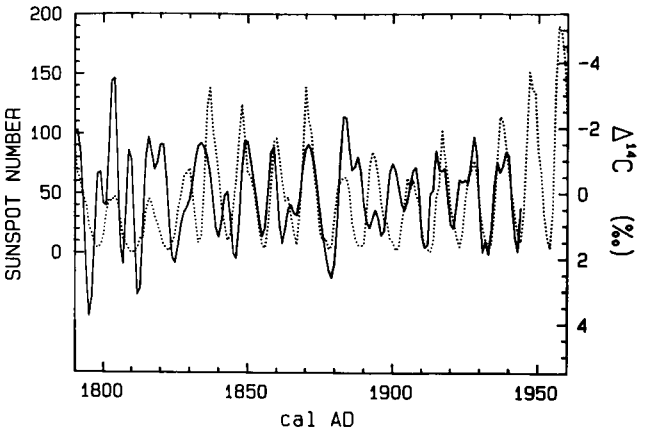

Figure 3a Filtered (5–20-year band pass) $\Delta^{14}C$ signal (solid line) derived from the Figure 1 data. The inverted $\Delta^{14}C$ signal is compared to unfiltered sunspot numbers (dotted line). For comparison purposes we reduced the $\Delta^{14}C$ cal ages by 4 years (see text). The vertical scales were arranged so that the post-AD 1715 means (and variances) of the respective time series plot equivalently.

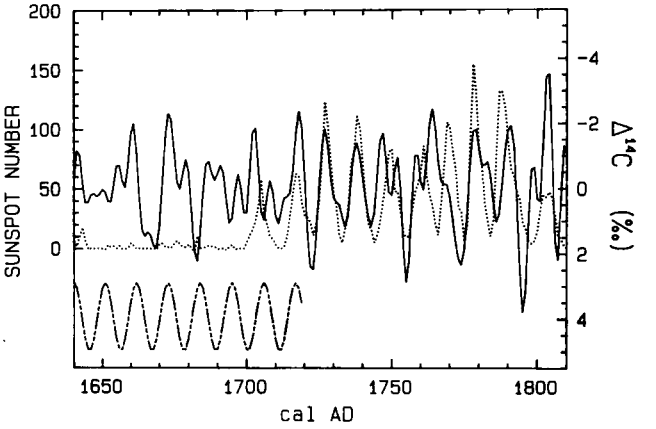

Figure 3b Similar to Figure 3a. An artificial 11-year cycle (lower dashed curve) was generated for the Maunder Minimum (AD 1650–1715).

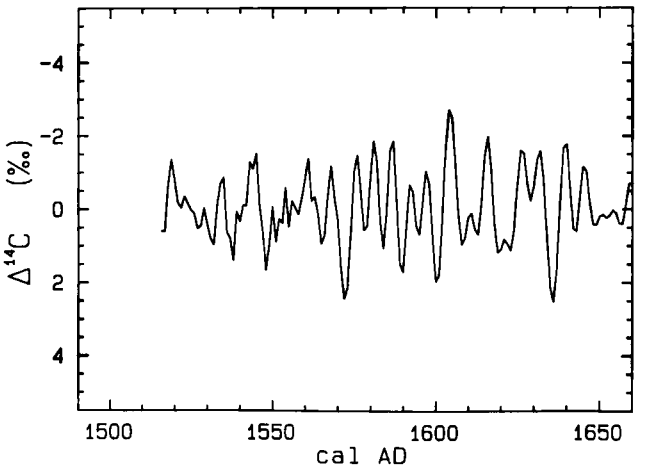

Figure 3c Filtered (5–20-year band pass) $\Delta^{14}C$ signal (solid line). Here the 4-year shift of Figures 3a and 3b was not applied but the inverted scale is retained. The available sunspot numbers for this interval are too disjointed for plotting.

simulated 11-year sinusoidal production rate changes of maximally 25%. The production rate changes for ^{10}Be, which has an atmospheric residence time of 1–2 years, are much less attenuated and the ^{10}Be concentration of polar ice (Dye 3, Greenland) has 11-year concentration changes in the 15–35%

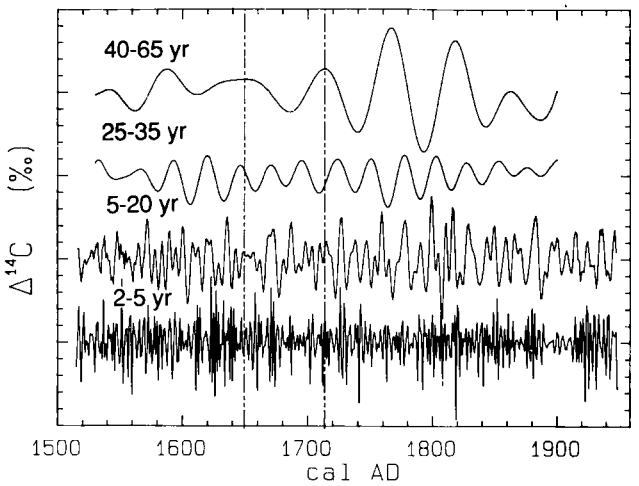

Figure 4 Filtered $\Delta^{14}C$ signals of the Figure 1 single-year record, using a split cosine band pass filter that passes the 56-year (top curve), 26-year, 11-year and 5-year (lower curve) periodicities as part of the ranges identified in the figure. Each tick mark on the vertical axis represents 1‰ and each curve is centred on a major tick. The lack of response for the higher frequencies near AD 1900 is due to the use of 2–3-year samples. The Maunder Minimum (AD 1650–1715) is indicated by the vertical dashed lines.

range (Beer *et al.*, 1990). These ^{10}Be concentration changes in ice (Beer *et al.*, 1990) of the AD 1780–1900 interval are compared in Figure 5a to the ^{14}C production rate changes (Q), calculated from the Figure 1 $\Delta^{14}C$ record through carbon reservoir (Braziunas, 1990; Stuiver and Braziunas, 1988) modelling. Variations are found to be approximately equal for measured ^{10}Be and calculated ^{14}C production, which agrees with the concept of a common (solar modulation of the cosmic ray flux) origin.

The largest correlation coefficient r between the ^{10}Be and Q data sets (3-year moving averages) for the AD 1640–1950 interval is 0.42, when ^{10}Be lags Q by 1.5 years (an extended ^{10}Be ice core data set was kindly provided for this comparison by J. Beer of the ETH, Zürich). This lag agrees with the 1–2-year residence time of ^{10}Be in the atmosphere. The possibility of finding these correlation coefficients for unrelated events is 1.4%. Although these numbers confirm that heliomagnetic modulation of cosmogenic isotope production is a common denominator in both records, only 18% of the variance in the records can be explained in this manner. Other variables, such as climate and continental dust, evidently play a major role in either the ^{10}Be or ^{14}C variance, or both.

The filtered (5–20-year) ^{10}Be and Q records are compared in Figure 5b. Here the correlation coefficient is lower ($r = 0.20$), due to the removal of longer-term trends, but the ^{10}Be–Q lag is the same 1.5 years as noted above. Despite the low r value, many increases in relative ^{10}Be concentration are seen to correspond to increases in relative Q of 1.5 years earlier; 10 out of 16 major ^{10}Be peaks and 10 out of 21 Q peaks match when accounting for the stated lag.

In the above analysis we find a 2.8‰ modulation for the eighteenth- and nineteenth-century 11-year cycle (average $\Delta^{14}C$ amplitude of the filtered record is 1.40 ± 0.16‰; for individual cycles $\sigma = 0.7$ per mil) in Pacific northwest trees. This amplitude differs significantly from the 4.8 ± 0.6 per mil found for Russian trees (Kocharov, 1992) for the AD 1600–1950 interval. Both records are compared in Figure 6. Considering the relatively fast mixing of CO_2 in the lower troposphere, on the order of months within each hemisphere and much faster zonally (Pearman and Hyson, 1980), the

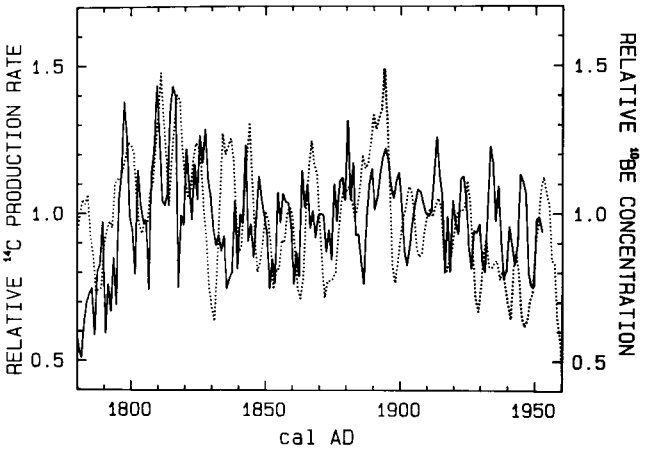

Figure 5a Relative ^{14}C production rate Q (solid line), calculated from the Figure 1 $\Delta^{14}C$ record through carbon reservoir modelling, compared to observed (no lag was applied) ^{10}Be concentration in polar ice (Beer, Blinov *et al.*, 1990). Each time series is plotted relative to its mean value.

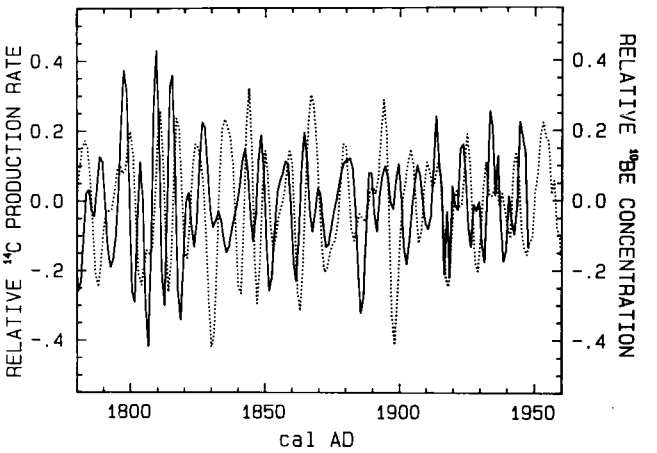

Figure 5b Similar to Figure 5a, except both the Q and ^{10}Be records were filtered with a 5–20-year split cosine band pass.

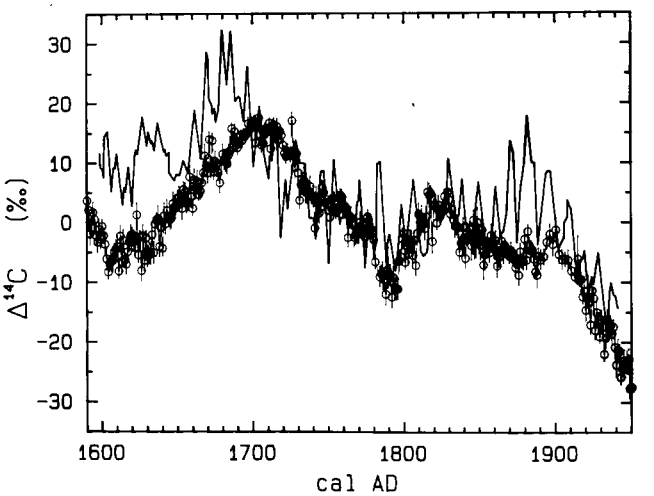

Figure 6 Single-year $\Delta^{14}C$ records of the Pacific northwest (circles) and Russia (solid line – Kocharov, 1992). The standard deviations of the Pacific northwest and Russian measurements are, respectively, about 2‰ and 2–3‰.

difference in 11-year cycle modulation is substantial, and difficult to explain. The larger modulation is also not supported by other observations. The appreciable 11-year modulation at high latitudes that was suggested previously for AD 1870–1885 tree-rings from the McKenzie River Region

(Fan *et al.*, 1986) has not been confirmed by recent measurements (Damon *et al.*, 1992). In addition, tentative results of GCM-based atmospheric tracer modelling by one of us (TFB) of the $^{14}CO_2$ 11-year cycle yielded an amplitude of 1.5 per mil (in good agreement with our Pacific northwest results) with only insignificant latitudinal differences in the northern hemisphere.

The sunspots, and related atmospheric ^{14}C production rate histories, have a strong imprint of the 11-year cycle that ultimately produces a rather small 11-year peak to trough (i.e., twice the amplitude) modulation of atmospheric $\Delta^{14}C$ of 2.8 per mil. At higher frequencies, production rate changes are even more attenuated in the atmospheric carbon reservoir (e.g., Houtermans *et al.*, 1973). At these higher frequencies, Kane (1977) identifies 18 sunspot periodicities in the 9.6–2.6-year range. Because the 11-year cycle dominates in the sunspot record, production rate changes associated with higher frequencies of the sunspot record must be appreciably smaller than those associated with the 11-year cycle. Given the small demonstrated 11-year $\Delta^{14}C$ modulation, it is unlikely that a substantial fraction of the Figure 1 $\Delta^{14}C$ variance in the 2–6.4-year range is directly associated with production rate change. However, solar production rate modulation could have played a role at the 13-, 17-, 26- and 56-year periodicities where atmospheric $\Delta^{14}C$ attenuation is less. Here Kane (1977) identifies 12.7-, 16.8-, 20.4-, 33.5- and 68-year periodicities in the sunspot record.

As noted above, other factors such as climate must contribute substantially to the variability of the single-year ^{10}Be and ^{14}C records. The ^{10}Be and ^{14}C production in the atmosphere is latitude dependent. Whereas tropospheric mixing of $^{14}CO_2$ is sufficiently fast to create nearly uniform ^{14}C concentrations in the atmosphere, ^{10}Be concentrations of the aerosols found in atmospheric precipitation show a distinct latitudinal gradient, reflecting a dependency on both regional climate and latitudinal production rate. Thus the climatic influence on the ^{10}Be concentration record in ice will be related to air mass transport mixing changes (and continental dust transport). Climatic influences on the $\Delta^{14}C$ record can be expected as well, but involve variations on a global scale related to atmospheric exchanges with other carbon reservoirs. Here a major contender for atmospheric $\Delta^{14}C$ change is oceanic circulation change, possibly synchronous with climate variation (ocean mode $\Delta^{14}C$).

Variable rates of upwelling associated with El Niño–Southern Oscillation (ENSO) events induce surface ocean $\Delta^{14}C$ variability (Brown *et al.*, 1993; Druffel, 1981). The cold phase of the ENSO cycle is associated with the upwelling of ^{14}C-deficient waters. The intra-annual, and 1972 ENSO related (measured for the 1970–1972 interval), $\Delta^{14}C$ change, registered by corals at the Galapagos Islands, is in the 35–50 per mil range (Brown *et al.*, 1993). Large amounts of nuclear bomb radiocarbon were advected into the mixed and thermocline layers of the oceans after AD 1954, and the ENSO $\Delta^{14}C$ signal in tropical waters under natural (prebomb) conditions must have been appreciably smaller. We estimate $\Delta^{14}C$ ENSO variations to have been in the 9–12 per mil range under natural conditions. Atmospheric $\Delta^{14}C$ also reflects exchange with the entire surface global ocean, of which substantial portions do not exhibit distinct ENSO ^{14}C property change. The ENSO affected air–sea exchange comprises about 10% of the total atmosphere/ocean exchange rate, thus indicating a natural atmospheric ENSO $\Delta^{14}C$ signal of about 1 per mil. Thus part of the variance associated with the 2–6.4-year periodicities observed in our atmospheric $\Delta^{14}C$ record (with $\Delta^{14}C$ amplitude about 1 per mil – see Figure 4) may relate to ENSO thermohaline circulation change.

Although the 2–6.4-year periodicities in the $\Delta^{14}C$ record correspond in duration to the irregular cycle of ENSO events (Cane and Zebiak, 1985; Cane *et al.*, 1986), a preliminary comparison of the timing of ENSO events (Quinn and Neal, 1992) shows minimal correlation with atmospheric $\Delta^{14}C$ digressions. Regional differences in annual tree-ring ^{14}C, however, may reflect ENSO related oceanic shifts (Jirikowic and Kalin, 1993).

The North Atlantic ocean's thermohaline circulation is driven by freshwater and heat supply to the mixed layer of the ocean. The intensity of the thermohaline circulation determines poleward heat transport, and influences global climate. Decadal/interdecadal variability in the North Atlantic air–sea–ice climate system has been attributed to P–E (the difference between precipitation and evaporation) forcing (Broecker *et al.*, 1990; Weaver *et al.*, 1991). Irregular thermohaline circulation oscillations of approximately 40–50 years were noticed by Delworth *et al.* (1993) in a coupled ocean–atmosphere model. The thermohaline intensity changes result globally in variable rates of upwelling of thermocline (^{14}C-deficient) waters and influence surface ocean $\Delta^{14}C$ values. This 'salt oscillator' mechanism, regionally distinct from ENSO but influencing $\Delta^{14}C$ in a similar manner, may have contributed to the global ocean mode $\Delta^{14}C$ on all timescales including the 2–56-year range. Of course, any postulated, ocean mode 10–11-year periodicity would have been masked or enhanced by the solar influence on $\Delta^{14}C$.

Centurial and millennial $\Delta^{14}C$ change

The discussion of 80-year and longer periodicities is tied to the extended tree-ring $\Delta^{14}C$ record, as derived by Stuiver and Reimer (1993) from the data of Kromer and Becker (1993), Linick *et al.* (1986), Pearson and Stuiver (1993) and Stuiver and Pearson (1993). Figures 7 and 8 include the atmospheric $\Delta^{14}C$ record derived from bidecadal tree-ring samples back to 11 390 cal. (calibrated) years BP (0 years BP = AD 1950). The tree-rings of the German oak chronology are dendrodated back to 9850 cal. years BP. An early Holocene pine chronology from south central Europe (Kromer and Becker, 1993) was used for the remaining portion of the tree-ring

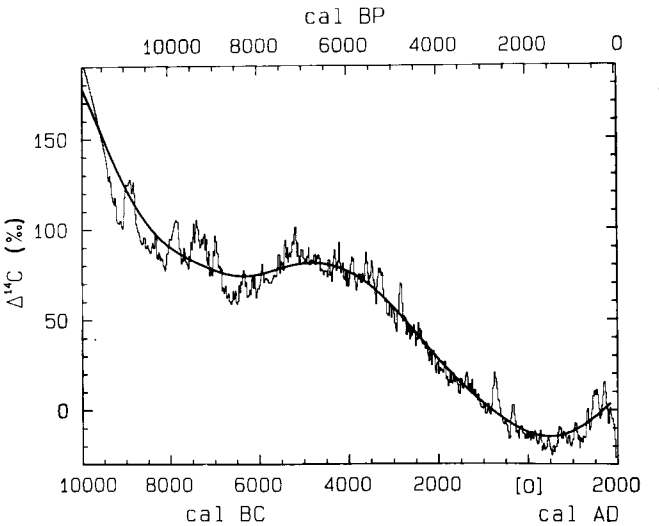

Figure 7 Atmospheric $\Delta^{14}C$ (coral-derived for the earliest 500 years, tree-ring derived for the remaining part) for the past 12 000 years. The long-term $\Delta^{14}C$ spline (smooth solid line), calculated from a ^{14}C production spline (Stuiver and Braziunas, 1993), resembles a 2000-year moving $\Delta^{14}C$ average.

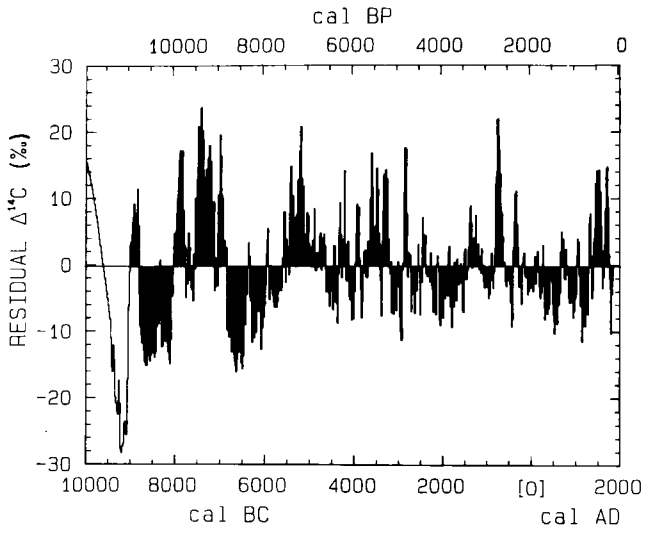

Figure 8 Residual $\Delta^{14}C$ obtained by deducting the Figure 7 long-term trend. Positive and negative values are shaded black, except for the oldest oscillation which is partly (first 500 cal. years) derived from coral determinations. The remaining $\Delta^{14}C$ values were derived from tree-ring measurements and do not include the recent anthropogenic (post-AD 1850) portion of the atmospheric record. Lowest $\Delta^{14}C$ value for the post-YD (Younger Dryas) oscillation is at 9190 BC (11 140 cal. years BP); the subsequent rapid $\Delta^{14}C$ increase (duration *c.* 150 years) starts at 9060 BC (11 010 cal. years BP). The eighteenth-century $\Delta^{14}C$ maximum is associated with the Maunder sunspot minimum.

based $\Delta^{14}C$ curve. The oldest part of the absolute German oak chronology, and the youngest portion of the pine chronology, have not yet been perfectly matched. The Kromer and Becker (1993) estimates of the pine–oak gap, resulting in absolute ages for the pine series, have been incorporated in the Figures 7 and 8 timescale. Other gap estimates, those by Bard *et al.* (1993) and Stuiver *et al.* (1991), would add, respectively, another 75 and 225 years to the cal. ages of the pine chronology.

A spline through the coral based ^{14}C ages (corrected by 400 ^{14}C years for the surface ocean reservoir age) associated with U/Th age determinations of Bard *et al.* (1993) yielded the Figures 7 and 8 pre-11 400 cal. BP curves. The matching of the marine and atmospheric information, and the pre-12 000 BP extension of the $\Delta^{14}C$ curve, are detailed in Bard *et al.* (1993) and Stuiver and Braziunas (1993). The long-term trend in the $\Delta^{14}C$ record can be determined in various ways (sine equations, moving averages, splines, etc.). Here we elected to use a Holocene production rate spline (see Stuiver and Braziunas, 1993) and calculated the Figure 7 atmospheric $\Delta^{14}C$ trend. This trend also strongly resembles a 2000-year moving average of $\Delta^{14}C$.

Strong arguments can be made that most of the long-term $\Delta^{14}C$ trend of the past 20 000 years relates to production rate variations tied to geomagnetic dipole intensity change (Bard *et al.*, 1990; Stuiver *et al.*, 1991; Mazaud *et al.*, 1991). The long-term $\Delta^{14}C$ trend is incompatible with sole oceanic forcing as an alternative (e.g., Stuiver and Braziunas, 1993). Of course, a significant portion of the variability in the long-term record could still relate to climatic (oceanic) or solar change. We elected, as a first approximation, to remove the putative geomagnetic component of the $\Delta^{14}C$ record by deducting the long-term spline. Figure 8 depicts the residual $\Delta^{14}C$ component of the record.

Power spectral densities of the residual $\Delta^{14}C$ record are given in Figures 9a and 9b. Periods exceeding the 2σ significance level in our Fourier analysis are 512 years, 206 years,

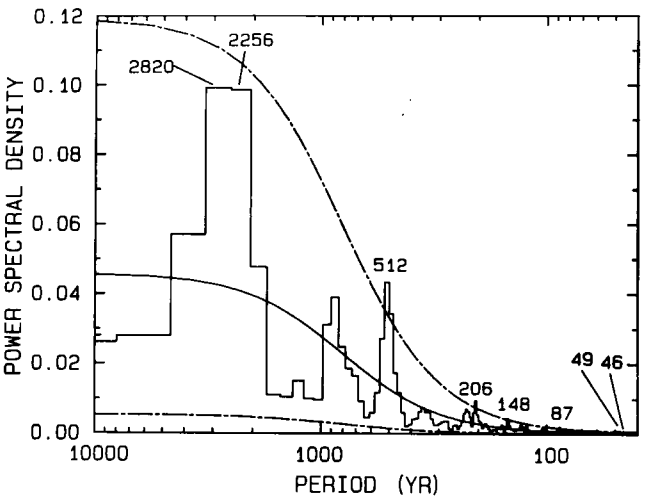

Figure 9a Power spectral density (PSD), obtained for the Figure 8 residual tree-ring $\Delta^{14}C$ record from Fourier power spectrum analysis (Mitchell *et al.*, 1966). The periods are given in years for each individual peak. The time interval analysed was 9440 BC–AD 1840. A maximum lag of 282 (half the number of data points) was applied.

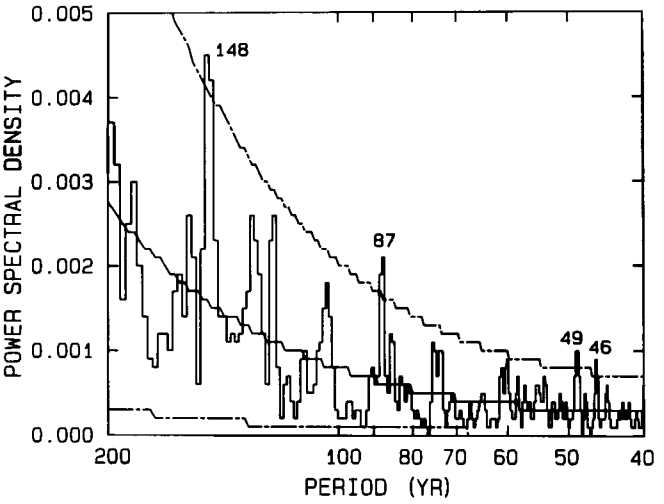

Figure 9b Expanded details of Figure 9a PSD spectrum.

148 years, 87 years and 46–49 years. The last of these periods approach the 56-year periodicity previously determined for the much shorter single-year record. The 2200–2600-year periodicity, discussed by Hood and Jirikowic (1990) for a 7200-year long $\Delta^{14}C$ record, increases in length by a few hundred years and does not quite attain the 2σ significance level (Figure 9a). And whereas a relatively weak 420-year periodicity explains several harmonics of the $\Delta^{14}C$ record (Stuiver and Braziunas, 1989), the 512-year cycle plays an important role here.

When investigating the spectral properties for intervals each lasting about 4000 cal. years, we find that the 512-year spectral power is concentrated in the earliest (9440 BC–6000 BC) portion of the tree-ring record. Figure 10 gives MEM spectral power for the three subintervals. As known, the MEM method produces well defined spectral peaks but the spectral power diagram does not accurately reflect the amplitude of the signals. Through Fourier analysis we determined 2σ or higher significance levels for the starred periodicities in Figure 10. Although 512-year periods are identified in both the 2000 BC–AD 1840 and the 9400 BC–6000 BC intervals, only the latter has significance beyond the 2σ level (at 99% significance level, versus 75% for the 2000 BC–AD 1840 interval).

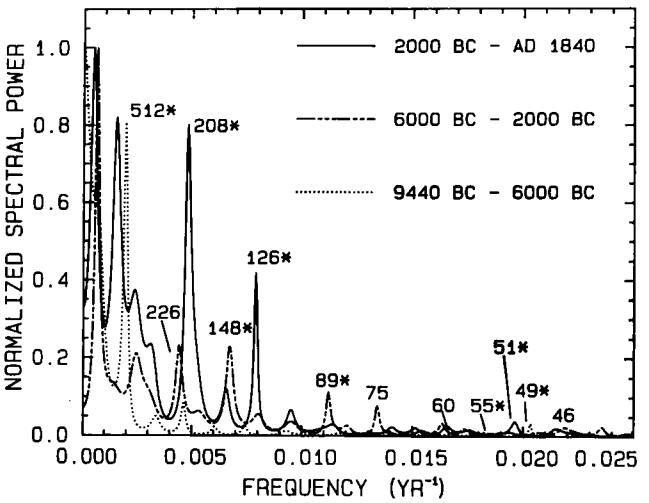

Figure 10 Relative power spectral density (PSD), normalized on the largest peak, obtained for specific intervals of the Figure 8 residual tree-ring $\Delta^{14}C$ record from MEM (maximum entropy method) using the Burg algorithm with an autoregressive (AR) order of 25% of the length of the data record. The periods are given in years for each individual peak. The confidence limits of the 208–226-year (206 and 225 years in the complete record) peaks are 99.9%, 90% and 85% for, respectively, the 2000 BC–AD 1840, 6000 BC–2000 BC and 9440 BC–6000 BC intervals. Starred periodicities denote significance levels exceeding two sigma confidence limits.

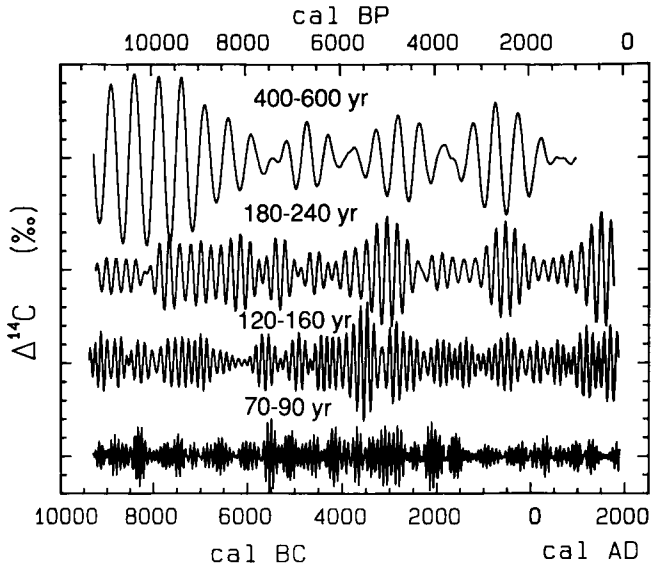

Figure 11a Filtered signals of the Figure 7 residual $\Delta^{14}C$ record, using a split cosine band pass filter centred (from top to bottom) on the 512-year, 206- (and 226-) year, 148- (and 126-) year and 87-year periodicities. The band pass widths are, respectively, 400–600 years, 180–240 years, 120–160 years, and 70–90 years. Each tick mark on the vertical axis represents 2‰ and each curve is centred on a major tick.

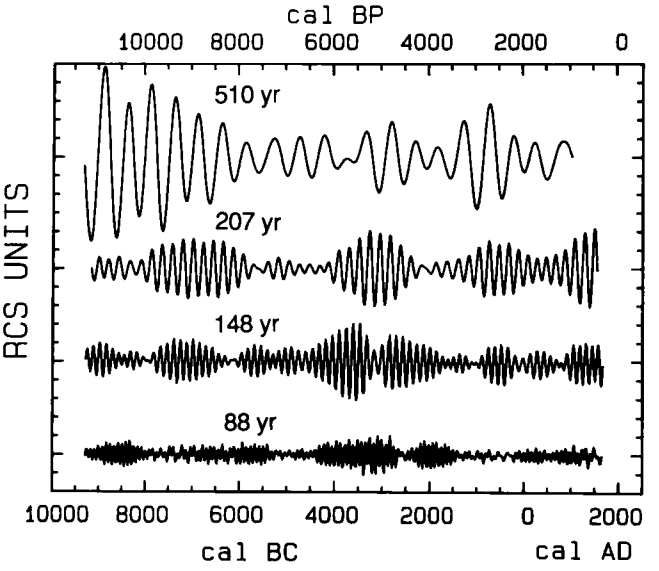

Figure 11b Singular spectrum analysis of the Figure 7 residual $\Delta^{14}C$ record (Ghil and Vautard, 1991). Reconstructed components (RCS) units are dimensionless. Approximate magnitude of $\Delta^{14}C$ change can be estimated from the ordinate of Figure 11a.

Focusing on the 512-year, 206- (and 226-) year, 148- (and 126-) year, and 87-year periods, we filtered the Figure 7 $\Delta^{14}C$ record with a split cosine band pass with widths of 400–600 years, 180–240 years, 120–160 years, and 70–90 years. The results are depicted in Figure 11a. We note that the filtered signal centred on the 512-year oscillation has the characteristics of a damped oscillation whereas the variances of the other filtered records are distributed more evenly over the entire Holocene interval. The maximum $\Delta^{14}C$ amplitudes of these filtered components decline with increasing frequency (from about 9 to 2‰). Although the 512-year period is basically the sole contributor to the 400–600-year band width, in the other instances the band widths may include multiple spectral peaks. For example, the 120–160-year and 180–240-year band widths include, respectively, the 126- and 148-year and the 206- and 226-year periodicities. The interaction between those signals results in amplitude modulation of the filtered signal. Using a narrow band pass we also find substantial modulation of the individual periodicities, similar to that reported by Damon and Sonett (1992) for their 208-year signal.

Singular spectrum analysis (Vautard and Ghil, 1989; E.R. Cook *et al.*, 1993) yields the Figure 11b filtered signals for the 510-year, 207-year, 148-year and 88-year periodicities. Signal modulation is more pronounced than that found previously (Figure 11a) as the singular spectrum analysis represents a narrower band pass. The basic variance patterns are similar for both methods, except for the 88-year cycle, where the singular spectrum signal has more pronounced features. The time separation of the maxima in the 207-year signal ranges from 2200 years to 3800 years, suggesting quite variable modulation, if any, by the 2200–2600-year cycle.

Previously we identified four recurrent 'triplet' $\Delta^{14}C$ episodes (Stuiver and Braziunas, 1989). The timing of these triplets coincides with the sequence of 206–226-year cycle amplitude maxima in Figure 11a. Only the 88-year cycle is still prominent for the interval lacking major $\Delta^{14}C$ perturbations (3000–4500 cal. BP, Figures 7 and 8).

Arguments for solar modulation of the cosmic ray flux as primary agent for Holocene centurial type $\Delta^{14}C$ change have been presented previously (e.g., Stuiver *et al.*, 1991). Ocean circulation forcing of centurial scale atmospheric $\Delta^{14}C$ has also been proposed (e.g., Lal, 1985). The information pertinent to the extended $\Delta^{14}C$ record leads to the following discussion.

Oceanic forcing of atmospheric $\Delta^{14}C$

The earliest portion of the Figure 8 centurial type residual $\Delta^{14}C$ record lends itself best to a discussion of the oceanic influence. The postulated mechanism for oceanic $\Delta^{14}C$ change is via the (unstable) salt oscillator in the North Atlantic,

where salinity lowering results in increased water stratification and reduced deep water formation. The latter in turn parallels reduced upwelling of ^{14}C-deficient water elsewhere in the oceans, thus increasing surface ocean and atmospheric $\Delta^{14}C$ levels.

Figure 12b of Stuiver and Braziunas (1993) (based on a splined version of the Bard *et al.*, 1993, data) indicates a steep $\Delta^{14}C$ decline for the 12 300–11 140 cal. BP interval. This rapid $\Delta^{14}C$ decline reflects not only a postulated post-12 300 cal. BP increase in global rates of upwelling, but also the relatively low $\Delta^{14}C$ levels of waters of intermediate or deep depths that now return faster to the surface. The most recent part of the $\Delta^{14}C$ decline, starting at about 12 000 cal. BP, is given in Figures 7 and 8. The 12 300 cal. BP age places the start of the $\Delta^{14}C$ decline at Younger Dryas (YD) age. For the (ocean mode $\Delta^{14}C$) interpretation of the early part of the record, the position of the Younger Dryas termination (YDT) relative to the steep $\Delta^{14}C$ perturbation is important.

The YDT cal. age of the GISP-2 (Greenland Ice Sheet Project) core is estimated at 11 650 ± 250 and 11 550 ± 70 cal. BP, based on annual layer (cryo) counting of, respectively, the GISP (Taylor *et al.*, 1993; Alley *et al.*, 1993) and GRIP (Greenland Ice Core Project – Johnson *et al.*, 1993) core. Laminated sediments from a Polish lake (Rozanski *et al.*, 1992) yield a slightly younger, 11 000–11 700 cal. BP range, with a preferred value of 11 200 cal. BP. The duration of the Younger Dryas, from lake varve counts (Rozanski *et al.*, 1992) and cryo counts (Alley *et al.*, 1993), is estimated at 1300 years, which leads to a 12 950 cal. BP date for the start of the Younger Dryas (YDS) in the GISP core. The YDS and YDT boundaries are well defined since the warm–cold and cold–warm transitions take less than 50 years (e.g., Lehman and Keigwin, 1992). The YDT and YDS atmospheric ^{14}C dates for 11 650 and 12 950 cal. BP, when using a splined version (Stuiver and Reimer, 1993) of the Bard *et al.* (1993) coral data, are, respectively, 10 100 ± 60 and 11 000 ± 60 BP. Here the ±60 represents only the uncertainty (one standard deviation) in the calibration curve. The above ^{14}C ages for the YDS and YDT cal. ages have to be compatible with available ^{14}C ages of YDS and YDT boundaries.

Mangerud *et al.* (1974), in good agreement with the above ^{14}C ages, place the YDT and YDS boundaries at 10 000 and 11 000 BP in their proposed classification of Quaternary stratigraphy. The radiocarbon ages for the YDT and YDS boundary determined by Lehman and Keigwin (1992) on North Sea Benthic foraminifera (and corrected by 440 ^{14}C years for reservoir deficiency) are slightly older, at 10 510 ± 120 and 11 300 ± 120 BP (the last date was estimated using an actual age determination on nearby material of 11 160 ± 120 BP). Statistics and an error multiplier (Stuiver and Pearson, 1992) can be invoked to explain part of the ^{14}C age difference (YDT difference is 410 ± 135 (3.0σ) and YDS 300 ± 135 (2.2σ) ^{14}C years), but the offsets could also be due to improper ^{14}C reservoir age corrections of either the North Sea benthics or the Barbados corals, or both. A shift of the cryo and varve count towards older cal. age, within the quoted errors of a few centuries, is another possibility, but would lead to disagreements with the more classical ^{14}C dates for the boundaries.

A 10 010 ± 90 BP age determination on surface foraminifera for the very end of the Younger Dryas off Ireland (Duplessy *et al.*, 1992) supports the 10 100 ± 60 BP YDT date derived from the ice core and coral data.

The Younger Dryas event has been tied to a shut down, or a weaker flux, of North Atlantic deep water (NADW) formation and transport (Duplessy *et al.*, 1992; Broecker and Denton, 1989). According to Fairbanks *et al.* (1990) the YD is bracketed by two meltwater pulses, whose peaks are dated at approximately 14 000 and 11 300 cal. BP (Fairbanks *et al.*, 1992).

Reduced global upwelling of ^{14}C-deficient waters associated with a lesser NADW flow would cause a surface water (and atmospheric) $\Delta^{14}C$ increase during the Younger Dryas. However, according to the $\Delta^{14}C$ profile, the postulated Younger Dryas $\Delta^{14}C$ 'high' ends fairly early in the YD, at 12 300 cal. BP (with the YD placed at 12 950–11 650 cal. BP in the GISP core and at 12 500–11 200 cal. BP in the Polish varved lake). Thus the $\Delta^{14}C$ perturbation suggests the start of increased NADW formation in the first half of the YD, instead of near its termination as suggested for other scenarios (e.g., Broecker and Denton, 1989).

The Fairbanks *et al.* (1992) meltwater pulses, culminating near 14 000 and 11 300 cal. BP, are expected to exert an influence on the salt oscillator as well. Following the salinity – $\Delta^{14}C$ scenario, the 14 000 and 11 300 cal. BP meltwater episodes suggest reduced deep water formation and higher atmospheric $\Delta^{14}C$ values. The U/Th dates around 14 000 cal. BP are too few to define a $\Delta^{14}C$ increase properly, but such a postulated $\Delta^{14}C$ high could have ended at 12 300 cal. BP when deep water formation increased. Following the associated $\Delta^{14}C$ decline, a rapid $\Delta^{14}C$ increase (Figure 8) started at 11 010 cal. BP, with a $\Delta^{14}C$ maximum near 10 900 cal. BP. This maximum is perhaps a corollary of the second meltwater pulse. However, the timing of the $\Delta^{14}C$ rise at 11 000 cal. BP, versus 11 300 cal. BP for the meltwater maximum, suggests either an atmospheric $\Delta^{14}C$ response lagging the oceanic disturbance by 300 years, or dating inaccuracies of the order of at least a couple of hundred years. Dating inaccuracies may well play a role, as Edwards *et al.* (1993) place the second meltwater pulse near 10 900 cal. BP, in good agreement with the timing of the ^{14}C maximum. The brief cooler conditions, near the 9900–9600 BP interval, identified as YD-II in a high-resolution diatom record from the southeast Norwegian Sea (Karpuz and Jansen, 1992), coincide with the $\Delta^{14}C$ maximum at 10 900 cal. BP.

Reduced deep water formation with its concomitant reduction in northward heat transport evidently induced the YD-II climatic episode. This episode is part of the 512-year damped $\Delta^{14}C$ oscillation. This cooler episode may also be reflected in a $\delta^{18}O$ reduction that follows the YD/Preboreal transition by about 200 cryoyears (summit cores GISP, Taylor *et al.*, 1993; and GRIP, Johnson *et al.*, 1993). This match is not ideal, however, as the ice core cal. ages assigned to the $\delta^{18}O$ episode are in the 11 400–11 300 cal. BP range.

Duplessy *et al.* (1992) show the YD event to be associated with substantial synchronous salinity reductions in two cores off Ireland and Portugal. Synchronous salinity events are not found in these cores during the Holocene, although the cores off Portugal and Ireland have nonsynchronous salinity lows at 8130, 6830, 4180 and 2970 BP. We do not imply that all salinity events have to be associated with deep water formation change but note that the oldest event of lower salinity, at 9000–9100 cal. BP (8130 ^{14}C years), coincides with a time of higher residual $\Delta^{14}C$ and thus would be compatible with a short-term reduction in NADW water flow.

Atmospheric $\Delta^{14}C$ declines that approximate 1% per 80 years and last several centuries generate ^{14}C age plateaus in the ^{14}C age–cal. age curves. Sarnthein *et al.* (1993) discuss the 9600 and 10 000 ^{14}C-year age plateaus (which are caused by the $\Delta^{14}C$ declines in the early part of Figure 8) and observe that the contemporaneity of $\delta^{13}C$ excursions and ^{14}C age plateaus are compatible with increases in deep water circulation for the duration of these plateaus.

Carbon reservoir model calculations (e.g., Stuiver and

Braziunas, 1993) show atmospheric $\Delta^{14}C$ levels and ^{14}C age differences between the deep and surface ocean (as derived from benthic–planktonic (b–p) ^{14}C age differences) to be very sensitive to the rate of deep water formation. For instance, steady state model atmospheric $\Delta^{14}C$ for a diffusive ocean with eddy diffusion coefficient K_z of 1000 m^2 $year^{-1}$ (Siegenthaler and Joos, 1992) is 28% above that of an ocean with the same K_z value to which deep water formation (at a rate of 1.6 m $year^{-1}$, or about $20\times10^6 m^3 sec^{-1}$) has been added. The calculated b–p differences change from about 4000 years for the purely diffusive ocean to a more acceptable 1000 years for the ocean with deep water formation. A full off-on switch of global deep water circulation is not possible near the Younger Dryas, as the Pacific Ocean b–p record (e.g., Andrée *et al.*, 1986; Shackleton *et al.*, 1988; Stuiver and Braziunas, 1993) cannot accommodate millennial b–p changes much beyond 400 ^{14}C years. Such an upper limit for b–p ^{14}C age change yields in our global carbon reservoir model a 20% upper limit for changes in rate of deep water formation around 12 300 cal. BP.

The transient increase in atmospheric $\Delta^{14}C$, associated with a postulated 20% reduction in deep water formation during 1300 years (the Younger Dryas), is 30‰ in the model and peaks at the YDT. A full turn off of deep water formation for 1300 years produces a 150‰ $\Delta^{14}C$ increase in our model atmosphere at the YDT boundary, which is half-way to the steady state increase (280‰). After subtracting the long-term trend (Figure 7) ascribed to geomagnetic influences, which contributes to the full 150‰ post-YD atmospheric $\Delta^{14}C$ drop, we indeed find a residual 30–50‰ decline in atmospheric $\Delta^{14}C$ following the YDT (Figure 8).

The nature of the residual $\Delta^{14}C$ changes associated with the 512-year $\Delta^{14}C$ cycle (see prior section) between 12 000 and 8000 cal. BP (Figures 8 and 11) suggests NADW flux oscillations gradually decreasing in magnitude with an occasional reactivation near 5000 and 3000 cal. BP. The 512-year cycle approximates the 600-year periodicity found in the molecular record of secular sea surface changes found for glacial terminations I, II and IV (Eglinton *et al.*, 1992). As noted by Eglington *et al.*, the sea surface temperature oscillations may be linked, in part, to abrupt break downs in Atlantic deep water ventilation resulting from meltwater events. Therefore the damped 512-year $\Delta^{14}C$ oscillation may represent the last phase of these Quarternary glacial termination events.

Increased oceanic circulation variance in the 320-year range has been observed in the Hamburg ocean general circulation model when driven by a white-noise freshwater flux superimposed on climatological fluxes (Mikolajewicz and Maier-Reimer, 1990). The Figure 9a spectral distribution shows some variance near 380 years but the surrounding 512- and 206-year peaks dominate. The period of the Hamburg model oscillation is determined by the advective timescale of the Atlantic circulation and could change for periods with thermohaline circulation differing from the present. If the observed 512-year cycle is related to such an internal oceanic oscillation, it would indicate reduced Atlantic thermohaline circulation for the early Holocene (about 320/512 or 0.6 times the present).

Whereas a strong 512-year $\Delta^{14}C$ oscillation is found in the early Holocene, the remaining part of the record is dominated by the 206-year cycle. Having assigned the 512-year oscillation to salinity changes one has to consider the possibility that the Holocene 206-year oscillations are tied to this mechanism as well. Such a direct ocean mode $\Delta^{14}C$ interpretation, however, is not supported by solar forcing considerations presented previously (Stuiver and Quay, 1980).

Solar forcing of centurial type $\Delta^{14}C$

Switching to a discussion of sun mode $\Delta^{14}C$, we now focus on the youngest part of the Figure 8 record, where the AD 1650–1715 Maunder sunspot minimum coincides with a $\Delta^{14}C$ maximum. The near zero sunspot number deduction agrees with the increased atmospheric $\Delta^{14}C$ levels found for the AD 1650–1715 interval, since cosmogenic isotope production rates increase for lesser sunspot numbers. Furthermore, a substantial increase in polar ice concentrations of ^{10}Be, another solar modulated cosmogenic isotope, occurs during the AD 1695–1710 interval (J. Beer, pers. comm.). Eleven-year cycle modulation of the solar wind (and cosmic ray flux) may have occurred during the Maunder Minimum even in the absence (or near absence) of sunspots as demonstrated by the Figure 3b single-year $\Delta^{14}C$ record, and by ^{10}Be ice core profiles (J. Beer, pers. comm.). Aurorae observations during the Maunder minimum (Schröder, 1988) also seem to possess an 11-year cycle component. Eleven-year cycle solar wind modulation was evidently still possible for a sun lacking sunspots.

By using the twentieth-century observed relationship between the 11-year cycles in atmospheric neutron production rate (which in turn is proportional to ^{14}C production rate) and sunspot numbers, the changes in ^{14}C production rate during the Maunder Minimum can be calculated. When accepting the premise of near zero sunspot numbers for the Maunder Minimum, the calculated $\Delta^{14}C$ Maunder Minimum increase is only half the observed one (Stuiver and Quay, 1980). The Maunder $\Delta^{14}C$ amplitude discrepancy can be removed, however, when postulated long-term trends in solar modulation are taken into account (Stuiver and Quay, 1980). The solar modulation considerations of Lal (1992), however, would limit the maximum ^{14}C production rate change during the Maunder minimum to about two-thirds of the increase needed to generate the observed $\Delta^{14}C$ increase in carbon reservoir models.

The magnitude of centurial type ^{10}Be ice core concentration change also agrees with such a solar mediated production rate change (Beer *et al.*, 1988a; 1988b; 1991; Stuiver *et al.*, 1991). However, as noted above, some of the higher frequencies of the single-year $\Delta^{14}C$ record, and the 512-year periodicity in the bidecadal $\Delta^{14}C$ record, appear to relate to oceanic causes. Thus the notion of a climate/ocean contribution for part of the centurial type $\Delta^{14}C$ oscillations cannot *a priori* be discarded.

Disregarding the remote possibility that the limited sunspot number observations during the Maunder Minimum have led us astray, we conclude that solar modulation of the cosmic ray flux explains at least half of the Maunder sun mode $\Delta^{14}C$ increase. The remaining half can be attributed either to additional cosmic ray flux increases when sunspots are absent (Stuiver and Quay, 1980), or to oceanic influences. As an alternative to the 100% solar origin for the Maunder $\Delta^{14}C$ maximum, we will explore below the possibility of an oceanic addition to the sun mode $\Delta^{14}C$.

If climate related oceanic circulation change plays a role it must enhance the Maunder $\Delta^{14}C$ signal. Hence a postulated mechanism is reduced upwelling (and deep water formation) during sun induced episodes of climatic change. Such sun–ocean mode $\Delta^{14}C$ differs from ocean mode $\Delta^{14}C$, where the $\Delta^{14}C$ change is induced solely by the global ocean.

Solar forcing evidently played a major role in generating the 206-year cycle. This cycle incorporates major aspects of the Maunder (and Spörer) type sunspot episodes. The 88-year cycle, already recognized by Gleissberg (1944) in the sunspot index, is also clearly tied to sun mode $\Delta^{14}C$. Similarly, the

130-year periodicity identified by Attolini *et al.* (1988) in records of historical aurorae suggests sun mode contributions to the Figure 11a variance in the 120–160-year range as well (as discussed in Stuiver, Braziunas, Becker and Kromer, 1991).

A possible sun–ocean contribution to atmospheric $\Delta^{14}C$

The residual $\Delta^{14}C$ variations so far have been tied to either ocean circulation change (ocean mode $\Delta^{14}C$) or solar modulation of atmospheric ^{14}C production (sun mode $\Delta^{14}C$). The possibility of a simultaneous contribution by both factors (sun–ocean mode $\Delta^{14}C$), where presumably solar forcing results in climatic change which in turn causes ocean circulation change, remains to be explored.

So far we have discussed the early Holocene 512-year oceanic (ocean mode $\Delta^{14}C$) and the seventeenth-century Maunder type (where at least half, and perhaps more, of the total is sun mode $\Delta^{14}C$) solar components of the $\Delta^{14}C$ record. Could there, especially for the 206-year cycle, be a pure or partial oceanic explanation for the remaining part of the Holocene $\Delta^{14}C$ record? This cycle is dominated by many Maunder and Spörer type oscillations, each of which strongly resembles the prototype event of the seventeenth century (Stuiver and Braziunas, 1988).

The required oceanic changes to induce a full Maunder type $\Delta^{14}C$ oscillation are certainly large. Our carbon model simulations (Stuiver *et al.*, 1991) suggest a K_z (vertical eddy diffusion coefficient) reduction by half. Evidence for possible changes in rate of upwelling can be found in regional ^{14}C levels of the ocean's surface layer as well as in regional composition of planktonic foraminiferal faunas. In Figure 12 we tried to find a relationship between atmospheric $\Delta^{14}C$ and upwelling rates by comparing normalized atmospheric $\Delta^{14}C$ values to Talma's (1990) record of radiocarbon age (reservoir age) change of surface waters off the coast of South Africa. The reservoir age changes are expressed as ΔR, a parameter defined as a regional offset in reservoir age relative to the global ocean (Stuiver and Braziunas, 1993). The ΔR scale is inverted in Figure 12, as lower atmospheric $\Delta^{14}C$ values would be compatible with larger surface water (increased radiocarbon age) ΔR values if upwelling rates are the causal mechanism. Although there is agreement for the 750–500 BC interval, crosscorrelation of the entire record yields a correlation coefficient of only 0.23 (with a probability of no correlation of 44%).

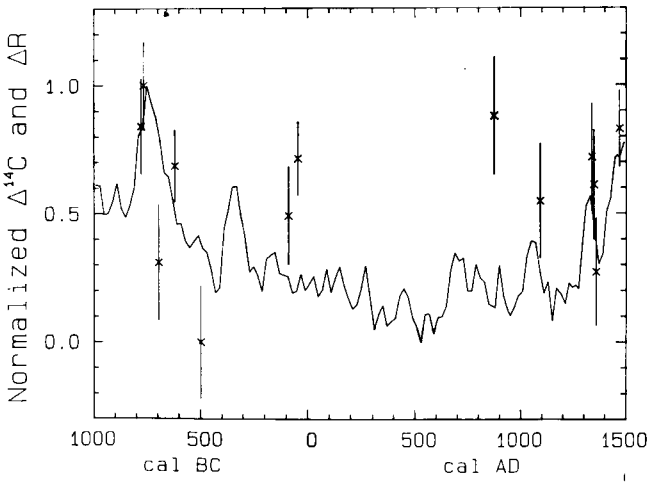

Figure 12 Atmospheric $\Delta^{14}C$ (solid line) values compared to reservoir ages ΔR (starred values with standard deviation). ΔR values are defined as regional offsets in surface ocean reservoir age relative to the time-dependent average reservoir age of the global surface ocean (Stuiver and Braziunas, 1993). The ΔR scale has been inverted; therefore reduced upwelling is represented by a larger ΔR value. Scales have been normalized so that the maximum range, and the averages, of the variables are identical.

A high-resolution study of planktonic foraminiferal faunas recovered from the Cariaco Basin in the southern Caribbean Sea (Peterson *et al.*, 1991) shows substantially variability in seasonal trade wind induced upwelling in this basin. The variance spectrum of *G. bulloides* contains concentrations of power in frequency bands (*c.* 420-, 218- and 143-year) similar to ^{14}C. The frequency bands are not well defined because the ^{14}C age calibration process leads to substantial uncertainties in the calibrated ages. Noting the spectral similarity of $\Delta^{14}C$ and faunal distribution, Peterson *et al.* (1991) suggest that solar forcing plays a role in the seasonal trade wind variability. However, the spectral agreement obtained (admittedly for certain timescale assumptions) may alternatively indicate a possible relationship between Holocene $\Delta^{14}C$ (centurial type) and ocean circulation change.

Pure oceanic forcing of all atmospheric centurial type $\Delta^{14}C$ is, in our opinion, unlikely because the Maunder $\Delta^{14}C$ discussion above shows that a substantial portion of this single $\Delta^{14}C$ event is already sun mode $\Delta^{14}C$. Previously we have advocated the sun mode $\Delta^{14}C$ component as being dominant in the centurial type $\Delta^{14}C$ record (Stuiver *et al.*, 1991; Stuiver and Quay, 1980), partly because for pure ocean mode forcing, very large (a factor of two) changes in deep water formation (and upwelling) were needed. For a postulated sun–ocean mode $\Delta^{14}C$ component, however, the required oceanic change would be substantially (at least one half) less. Here the sun would initiate the process (solar induced climate change) which ultimately results in ocean circulation change that amplifies the climate perturbation during Maunder type episodes of low sunspot numbers. If climate indeed plays a role in augmenting Maunder type $\Delta^{14}C$ perturbations, actual Maunder type cosmic ray changes will be less than those calculated for a full $\Delta^{14}C$ change. The ^{10}Be concentration can be influenced by climate as well. Good agreement is found between the magnitudes of calculated ^{14}C production rate changes and ^{10}Be concentration data when assuming zero climatic influence. Such agreement, however, would also have been observed for fortuitously equal climate contributions to both signals.

A solar influence on climate can only be deduced from climate–atmospheric $\Delta^{14}C$ considerations if these $\Delta^{14}C$ variations are dominated by solar mode $\Delta^{14}C$. Acceptance of the AD 1650–1715 Maunder episode of low sunspot numbers implies that at least half of the Maunder $\Delta^{14}C$ increase is solar mode $\Delta^{14}C$. Agreement of ^{10}Be and $\Delta^{14}C$ patterns (Beer *et al.*, 1990; Stuiver *et al.*, 1991) suggests a solar influence on several other Maunder (or longer Spörer) type perturbations as well. In the following discussion we adhere to the premise that centurial type $\Delta^{14}C$ (with the 512-year cycle excluded, see above) is composed of sun mode $\Delta^{14}C$, with possibly an oceanic contribution up to one half of the Maunder $\Delta^{14}C$ signal.

For sun–climate relationships the question of solar 'constant' change is of crucial importance. Changes of up to 0.06% have been measured for the recent 11-year sunspot cycle (Schatten, 1988; Wilson and Hudson, 1988). The increase in solar constant occurred when sunspot numbers S changed from 20 to 140. On a longer timescale, the absence of sunspots during the AD 1650–1715 Maunder Minimum can be compared to an average sunspot number of 51 for the recent AD 1880–1965 interval. By analogy, the solar constant

change between these periods would only be 51/120 $\times 0.06 = 0.026\%$.

The related global temperature variations for the Maunder Minimum are of the order 0.1–0.3°C (Gérard, 1990), far short of the drop in primarily European temperatures postulated for the 'Little Ice Age'. Clearly an amplification mechanism is required for tropospheric temperature change (e.g., van Loon and Labitzke, 1988, although statistically not foolproof). Here we explore a positive feedback mechanism involving perturbations of the inherently unstable North Atlantic salt oscillator.

The current 'Global Change' emphasis on high-resolution climate records has led to an improved understanding of centurial type climate change. Not all studies lead to the conclusion that $\Delta^{14}C$ and climate, or the sun and climate, are related (e.g., Stuiver, 1980; Pittock, 1978; 1983) but similarities between $\Delta^{14}C$ and regional climate have been noticed by Sonett and Suess (1984), Wigley and Kelly (1990), Anderson (1992), Taylor *et al.* (1992), Magny (1993), E. Cook *et al.* (1992; 1993) and Scuderi (1993). As an example we note the Magny study of lake level and climate change in the French Alps region. Here high lake level stands (increased precipitation and colder temperatures) are related to atmospheric $\Delta^{14}C$ maxima. Correlations of such variables, of course, need not always be proof of a causal relationship. However, in case $\Delta^{14}C$ and climate are indeed related, there are certain implications for the sun–climate–$\Delta^{14}C$ connection. As the climate–$\Delta^{14}C$ connection is open to debate, the causal relationship suggested below is very tentative.

We assume that for a prolonged state of near zero sunspot numbers (Maunder Minimum) the relatively minor reduction in solar constant produces a minor temperature reduction, and precipitation increase, for that part of the North Atlantic region where deep water formation is important. This would only be a regional effect as lower temperature, on a global scale, accompanies less precipitation (less water vapour is generated at the lower temperature). Magny's (1993) work suggests our Maunder minimum temperature–precipitation hypothesis to be applicable for parts of western Europe. Modelling efforts by Rind and Overpeck (1993) confirm the French study but do suggest that the temperature reduction–precipitation increase combination is not valid for the entire northern Atlantic region. As substantial uncertainties remain in regional climate modelling, this was not a compelling reason for us to discard our hypothesis.

The net effect of the minor climate and freshwater input change over several decades would be a lowering of surface ocean density in the north Atlantic region. The salinity lowering triggers change in the unstable north Atlantic thermohaline deep water circulation. The change will be towards less deep water formation, less upwelling, and less northward heat transport of the Gulf Stream (assuming that the effects of salinity lowering are not counteracted by increased sea ice cover associated with lower temperature). The resulting colder conditions in the north Atlantic region amplify the initial (solar induced) climate signal. As the rate of upwelling of ^{14}C-deficient waters will be reduced as well, the solar (zero sunspots) mediated atmospheric $\Delta^{14}C$ increase is also amplified.

Although the above hypothesis is compatible with the postulated climate–$\Delta^{14}C$ relationship, a different salt oscillator trigger could play a role too. As noted, the direct solar induced climate change in the troposphere is small when considering the solar constant change; yet the upper stratosphere experiences substantial decreases in ultraviolet (UV) radiation when sunspot numbers decrease. Plankton survival in the surface layer of the ocean depends inversely on UV radiation (Smith *et al.*, 1992; Herndl *et al.*, 1993), and a Maunder Minimum UV radiation decrease at the earth surface could increase plankton biomass by several per cent (although the relative percentage decrease in UV flux near the earth will be smaller than the percentage UV flux decrease in the upper atmosphere due to a reduction in ozone concentration – Brasseur *et al.*, 1987). Charlson *et al.* (1987) proposed that production of dimethylsulphide (DMS) by marine plankton is a major source of aerosol sulphate in the marine atmosphere, and, in turn, of cloud condensation nuclei. Increased precipitation would be the corollary of the increased plankton biomass, and thermohaline deep water formation in the north Atlantic would again be reduced due to the salinity reduction in its source regions. In a way analogous to the first scheme, the UV scenario results in a Maunder Minimum increase in rate of precipitation and a lowering of temperature due to a reduction in Gulf Stream heat transport.

The anthropogenic lowering of current stratospheric ozone concentrations increases UV levels near the earth's surface. The climatic consequences of this increase, if our hypothesis is valid, would be a reduction in precipitation rates and an enhancement of Gulf Stream heat transport, thus enhancing the greenhouse warming predicted for the near future.

The above hypothetical aspects of a sun–climate relationship are speculative in that a tendency of the thermohaline circulation to succumb to small input signals over several decades has not been proven. Furthermore, this mechanism would primarily change climate specifically of the north Atlantic region. Our suggestions are not final; they are only intended as a start for a further exploration of a possible sun–climate relationship.

Final notes

In our analysis we have emphasized the diversity of the causes contributing to the atmospheric $\Delta^{14}C$ record. Solar modulation of the cosmic ray flux and climate induced oceanic change are major players, the latter especially during the intervals preceding and immediately following the Younger Dryas–Preboreal boundary. An oceanic contribution during the early Holocene is evident in the damped 512-year $\Delta^{14}C$ oscillation. This oscillation is also important for radiocarbon age calibration, as it introduces major plateaus in the ^{14}C age–cal. age calibration curves. Although some recent studies of the relationship between climate and $\Delta^{14}C$ seem to suggest an interdependence, we are not impressed by the significance of these relationships, as the correlation coefficients are relatively low (Stuiver *et al.*, 1991). However, if such a relationship should exist, it has major consequences for the conceptual ideas underlying climate and $\Delta^{14}C$ forcing. Amplification of a weak solar signal is needed; such amplification is explored by us in speculative mechanisms involving UV and north Atlantic thermohaline circulation change. These mechanisms may lead to a potential oceanic contribution towards a solar induced Maunder type atmospheric $\Delta^{14}C$ change of up to one-third to one-half of the ultimate $\Delta^{14}C$ signal.

Acknowledgements

The ^{14}C research was supported through the National Science Foundation, and NOAA contract NA16RC00081. We are much indebted to E.R. Cook, Columbia University, for sup-

plying the singular spectrum computer program, to J. Beer, ETH Zürich, for providing single year ^{10}Be data for comparison with Δ^{14}C values, and to P.J. Reimer and P.J. Wilkinson for crucial technical and analytical support. The constructive reviewer remarks of J. Beer and P.M. Grootes are gratefully acknowledged. For JISAO, this is contribution number 206.

References

Alley, R.B., Meese, D.A., Shuman, C.A., Gow, A.J., Taylor, K.C., Grootes P.M., White, J.W.C., Ram, M., Waddington, E.D., Mayewski, P.A. and **Mielinski, A.G.** 1993: Abrupt increase in Greenland snow accumulation at the end of the Younger Dryas event. *Nature* 362, 527–29.

Anderson, R.Y. 1992: Possible connection between surface winds, solar activity and the Earth's magnetic field. *Nature* 358, 51–53.

Andrée, M., Beer, J., Loetscher, H.P., Moor, E., Oeschger, H., Bonani, G., Hofmann, H.J., Suter, M., Woelfli, W. and **Peng, T.H.** 1986: Limits on the ventilation rate for the deep ocean over the last 12000 years: *Climate Dynamics* 1, 53–62.

Attolini, M.R., Galli, M. and **Nanni, T.** 1988: Long and short cycles in solar activity during the last millennia. In Stephenson, F.R. and Wolfendale, A.W., editors, *Secular solar and geomagnetic variations in the last 10,000 years*, Dordrecht: Kluwer, 49–68.

Bard, E., Hamelin, B., Fairbanks, R.G. and **Zindler, A.** 1990: Calibration of the ^{14}C timescale over the past 30,000 years using mass spectrometric U-Th ages from Barbados corals. *Nature* 345, 405–10.

Bard, E., Arnold, M., Fairbanks, R.G. and **Hamelin, B.** 1993: ^{230}Th-^{234}U and ^{14}C ages obtained by mass spectrometry on corals. *Radiocarbon* 35, 191–99.

Beer, J., Siegenthaler, U. and **Blinov, A.** 1988: Temporal ^{10}Be variations in ice: information on solar activity and geomagnetic field intensity. In Stephenson, F.R. and Wolfendale, A.W., editors, *Secular solar and geomagnetic variations in the last 10,000 years*, Dordrecht: Kluwer, 297–314.

Beer, J., Raisbeck, G.M. and **Yiou, F.** 1991: The variations of ^{10}Be and solar activity. In Sonett, C.P., Giampapa, M.S. and Matthews, M.S., editors, *The Sun in Time*, Tucson: University of Arizona Press, 343–59.

Beer, J., Siegenthaler, U., Bonani, G., Finkel, R.C., Oeschger, H., Suter, M. and **Wölfli, W.** 1988: Information on past solar activity and geomagnetism from ^{10}Be in the Camp Century ice core. *Nature* 331, 675–79.

Beer, J., Blinov, A., Bonani, G., Finkel, R.C., Hofmann, H.J., Lehmann, B., Oeschger, H., Sigg, A., Schwander, J., Staffelbach, T., Stauffer, B., Suter, M. and **Wölfli, W.** 1990: Use of ^{10}Be in polar ice to trace the 11-year cycle of solar activity. *Nature* 347, 164–66.

Brasseur, G., De Rudder, A., Keating, G.M. and **Pitts, M.C.** 1987: Response of middle atmosphere to short-term solar ultraviolet variations: 2. Theory. *Journal of Geophysical Research* 92, 903–14.

Braziunas, T.F. 1990: Nature and origin of variations in late-glacial and Holocene atmospheric ^{14}C as revealed by global carbon cycle modeling. Ph.D. dissertation, University of Washington.

Broecker, W.S. and **Denton, G.** 1989: The role of ocean–atmosphere reorganization in glacial cycles. *Geochimica et Cosmochimica Acta* 53, 2465–501.

Broecker, W.S., Bond, G., Klaus, M., Bonani, G. and **Wölfli, W.** 1990: A salt oscillator in the glacial Atlantic? 1. The concept. *Paleoceanography* 5, 469–77.

Brown, T.A., Farwell, G.W., Grootes, P.M., Schmidt, F.H. and **Stuiver, M.** 1993: Intra-annual variability of the radiocarbon content of corals from the Galapagos Islands. *Radiocarbon* 35, 245–51.

Cane, M.A. and **Zebiak, S.E.** 1985: A theory for El Niño and the Southern Oscillation. *Science* 228, 1085–87.

Cane, M.A., Zebiak, S.E. and **Dolan, S.C.** 1986: Experimental forecasts of El Niño. *Nature* 231, 827–32.

Charlson, R.J., Lovelock, J.E., Andreae, M.O. and **Warren, S.G.** 1987: Oceanic phytoplankton, atmospheric sulfur, cloud albedo and climate. *Nature* 326, 655–61.

Cook, E., Bird, T., Peterson, M., Barbetti, M., Buckley, B., D'Arrigo, R. and **Francey, R.** 1992: Climatic change over the last millennium in Tasmania reconstructed from tree-rings. *The Holocene* 2, 205–17.

Cook, E.R., Buckley, B.M. and **D'Arrigo, R.D.** 1993: Decadal-scale oscillatory modes in a millennia-long temperature reconstruction from Tasmania. *Proceedings of the National Academy of Sciences Workshop on 'The natural variability of the climate system on 10–100 year time-scales'*, Irvine, Cal., 21–24 Sept. 1992, in press.

Damon, P.E. and **Sonett, C.P.** 1992: Solar and terrestrial components of the atmospheric ^{14}C variation spectrum. In Sonett, C.P., Giampapa, M.S. and Matthews, M.S., editors, *The Sun in Time*, Tucson: University of Arizona Press, 361–87.

Damon, P.E., Burr, G., Cain, W.J. and **Donahue, D.J.** 1992: Anomalous 11-year Δ^{14}C cycle at high latitudes? *Radiocarbon* 34, 235–38.

Delworth, T., Manabe, S. and **Stouffer, R.J.** 1993: Interdecadal variations of the thermohaline circulation in a coupled ocean–atmosphere model. *Journal of Climate*, in press.

Druffel, E.R.M. 1981: Radiocarbon in annual coral rings from the eastern tropical Pacific Ocean. *Geophysical Research Letters* 8, 59–62.

Duplessy, J.C., Labeyrie, L., Arnold, M., Paterne, M., Duprat, J. and **van Weering, T.C.E.** 1992: Changes in surface salinity of the North Atlantic Ocean during the last deglaciation. *Nature* 358, 485–88.

Eddy, J.A. 1976: The Maunder Minimum. *Science* 192, 1189–202.

Edwards, R.L., Beck, J.W., Burr, G., Donahue, D., Chappell, J.M.A., Bloom, A.L., Druffel, E.R.M. and **Taylor, F.W.** 1993: A large drop in atmospheric ^{14}C/^{12}C and reduced melting in the Younger Dryas, documented with ^{230}Th ages of corals. *Science* 260, 962–68.

Eglinton, G., Bradshaw, S.A., Rosell, A., Sarnthein, M., Pfaumann, U. and **Tiedemann, R.** 1992: Molecular record of secular sea surface temperature changes on 100-year timescales for glacial terminations I, II, and IV. *Nature* 356, 423–26.

Fairbanks, R.G. 1990: The age and origin of the 'Younger Dryas climate event' in Greenland ice cores. *Paleoceanography* 5, 937–48.

Fairbanks, R.G., Charles, D.C. and **Wright, J.D.** 1992: Origin of global meltwater pulses. In Taylor, R.E., Long, A., and Kra, R.S., editors, *Radiocarbon After Four Decades*, New York: Springer-Verlag, 473–500.

Fan, C.Y., Chen, T.M., Yun, S.X. and **Dai, K.M.** 1986: Radiocarbon activity variation in dated tree rings grown in McKenzie Delta. *Radiocarbon* 25, 205–12.

Gérard, J.-C. 1990: Modelling the climate response to solar variability. *Philosophical Transactions of the Royal Society of London* A 330, 561–74.

Ghil, M. and **Vautard, R.** 1991: Interdecadal oscillations and the warming trend in global temperature time series. *Nature* 350, 324–27.

Gleissberg, W. 1944: A table of secular variations of the solar cycle. *Terrestrial Magnetism and Atmospheric Electricity* 49, 243–44.

Herndl, G.J., Müller-Niklas, G. and **Frick, J.** 1993: Major role of ultraviolet-B in controlling bacterioplankton growth in the surface layer of the ocean. *Nature* 361, 717–19.

Hood, L.L. and **Jirikowic, J.L.** 1990: Recurring variations of probable solar origin in the atmospheric Δ^{14}C time record. *Geophysical Research Letters* 17, 85–88.

Houtermans, J.C., Suess, H.E. and **Oeschger, H.** 1973: Reservoir models and production rate variations of natural radiocarbon. *Journal of Geophysical Research* 78, 1897–1907.

Jirikowic, J.L. and **Kalin, R.M.** 1993: A possible paleoclimatic ENSO indicator in the spatial variation of annual tree-ring ^{14}C. *Geophysical Research Letters* 20, 439–42.

Johnson, S.J., Clausen, B., Dansgaard, W., Fuhrer, K., Gundestrup, N., Hammer, C.U., Iversen, P., Jouzel, J., Stauffer, B. and **Steffenson, J.P.** 1993: Irregular glacial interstadials recorded in a new Greenland ice core. *Nature* 359, 311–13.

Kane, R.P. 1977: Power spectrum analysis of solar and geophysical parameters. *Journal of Geomagnetism and Geoelectricity* 29, 471–95.

Karpuz, N.K. and **Jansen, E.** 1992: A high-resolution diatom record of the last deglaciation from the SE Norwegian Sea: documentation of rapid climatic changes. *Paleoceanography* 7, 499–520.

Kocharov, G.E. 1992: Radiocarbon and astrophysical-geophysical

phenomena. In Taylor, R.E., Long, A. and Kra, R.S., editors, *Radiocarbon After Four Decades*, New York: Springer-Verlag, 130–45.

Kromer, B. and **Becker, B.** 1993: German oak and pine ^{14}C calibration, 7200–9400 BC. *Radiocarbon* 35, 125–35.

Lal, D. 1985: Carbon cycle variations during the past 50,000 years: atmospheric $^{14}C/^{12}C$ ratio as an isotopic indicator. In Sundquist, E.T. and Broecker, W.S., editors, *The carbon cycle and atmospheric CO_2: natural variations archean to present*, Washington, D.C.: American Geophysical Union, Geophysical Monograph 32, 221–33.

—— 1992: Expected secular variations in the global terrestrial production of radiocarbon. In Bard, E. and Broecker, W.S., editors, *NATO ASI Series 1, Global Environmental Change*, Volume 2, *The last deglaciation: absolute and radiocarbon chronologies*, Heidelberg: Springer-Verlag, 113–26.

Lehman, S.J. and **Keigwin, L.D.** 1992: Sudden changes in North Atlantic circulation during the last deglaciation. *Nature* 356, 757–62.

Lingenfelter, R.E. 1963: Production of carbon 14 by cosmic-ray neutrons. *Review of Geophysics* 1, 35–55.

Linick, W.L., Long, A., Damon, P.E. and **Ferguson, C.W.** 1986: High-precision radiocarbon dating of bristlecone pine from 6554 to 5350 BC. *Radiocarbon* 28, 943–53.

Magny, M. 1993: Solar influences on Holocene climatic changes illustrated by correlations between past lake-level fluctuations and the atmospheric ^{14}C. *Quaternary Research* 39, in press.

Mangerud, J., Andersen, S.T., Berglund, B.E. and **Donner, J.J.** 1974: Quaternary stratigraphy of Norden, a proposal for terminology and classification. *Boreas* 3, 109–28.

Mazaud, A., Laj, C., Bard, E., Arnold, M. and **Tric, E.** 1991: Geomagnetic field control of ^{14}C production over the last 80 ky: implications for the radiocarbon time-scale. *Geophysical Research Letters* 18, 1885–88.

Mikolajewicz, U. and **Maier-Reimer, E.** 1990: Internal secular variability in an ocean general circulation model. *Climate Dynamics* 4, 145–56.

Mitchell, Jr., J.M., Dzerdzeevskii, B., Flohn, H., Hofmeyr, W.L., Lamb, H.H., Rao, K.N. and **Wallen, C.C.** 1966: Climatic change. *World Meteorological Organization, Technical Note No. 79*, 79 pp.

O'Brien, K. 1979: Secular variations in the production of cosmogenic isotopes. *Journal of Geophysical Research* 84, 423–31.

Pearman, G.I. and **Hyson, P.** 1980: Activities of the global biosphere as reflected in atmospheric CO_2 records. *Journal of Geophysical Research* 85, 4457–68.

Pearson, G.W. and **Stuiver, M.** 1993: High-precision bi-decadal calibration of the radiocarbon time scale, 500–2500 BC. *Radiocarbon* 35, 25–33.

Peterson, L.C., Overpeck, J.T., Kipp, N.G. and **Imbrie, J.** 1991: A high-resolution late quaternary upwelling record from the Anoxic Cariaco Basin, Venezuela. *Paleoceanography* 6, 99–119.

Pittock, A.B. 1978: A critical look at long-term sun–weather relationships. *Review of Geophysics and Space Physics* 16, 400–20.

—— 1983: Solar variability, weather and climate: an update. *Quarterly Journal Royal Meteorological Society* 109, 23–55.

Quenouille, M.H. 1952: *Associated Measurements.* Vol. 68. London: Butterworths.

Quinn, W.H. and **Neal, V.T.** 1992: The historical record of El Niño events. In Bradley, R.S. and Jones, P.D., editors, *Climate since AD 1500*, London and New York: Routledge, Chapman and Hall, 623–48.

Rind, D. and **Overpeck, J.** 1993: Hypothesized causes of decade-to-century-scale climate variability: climate model results. *Quaternary Science Reviews*, in press.

Rozanski, K., Goslar, T., Dulinski, M., Kuc, T., Pazdur, M.F. and **Walanus, A.** 1992: The late glacial–Holocene transition in central Europe derived from isotope studies of laminated sediments from Lake Gosciaz (Poland). In Bard, E. and Broecher, W.S., editors, *NATO ASI Series 1, Global Environmental Change*, Vol. 2, *The last deglaciation: absolute and radiocarbon chronologies*, Heidelberg: Springer-Verlag, 69–80.

Sarnthein, M., Winn, K., Jung, S., Duplessy, J.-C., Labeyrie, L., Erlenkeuser, H. and **Ganssen, G.** 1993: Changes in east Atlantic deep-water circulation over the last 30,000 years – an eight-time-slice record. Submitted to *Paleoceanography.*

Schatten, K.H. 1988: A model for solar constant secular changes. *Geophysical Research Letters* 15, 121–24.

Schröder, W. 1988: Aurorae during the Maunder Minimum. *Meteorology and Atmospheric Physics* 38, 246–51.

Scuderi, L.A. 1993: A 2000-year tree ring record of annual temperatures in the Sierra Nevada mountains. *Science* 259, 1433–36.

Shackleton, N.J., Duplessy, J.-C., Arnold, M., Maurice, P., Hall, M.A. and **Cartlidge, J.** 1988: Radiocarbon age of last glacial Pacific deep water. *Nature* 335, 708–11.

Siegenthaler, U. and **Joos, F.** 1992: Use of a simple model for studying oceanic tracer distributions and the global carbon cycle. *Tellus* 44b, 186–207.

Smith, R.C., Prezelin, B.B., Baker, K.S., Bidigare, R.R., Boucher, N.P., Coley, T., Karentz, D., MacIntyre, X., Matlick, H.A., Menzies, D., Ondrusek, M., Wan, Z. and **Maters, K.J.** 1992: Ozone depletion: ultraviolet radiation and phytoplankton biology in Antarctic waters. *Science* 255, 952–59.

Sonett, C.P. and **Suess, H.E.** 1984: Correlation of bristlecone pine ring widths with atmospheric ^{14}C variations: a climate–sun relation. *Nature* 307, 141–43.

Stuiver, M. 1980: Solar variability and climatic change during the current millennium. *Nature* 286, 868–71.

—— 1982: A high-precision calibration of the AD radiocarbon time scale, *Radiocarbon* 24, 1–26.

—— 1993: A note on single-year calibration of the radiocarbon time scale, AD 1510–1954. *Radiocarbon* 35, 67–72.

Stuiver, M. and **Becker, B.** 1993: High-precision decadal calibration of the radiocarbon time scale, AD 1950–6000 BC. *Radiocarbon* 35, 35–65.

Stuiver, M. and **Braziunas, T.F.** 1988: The solar component of the atmospheric ^{14}C record. In Stephenson, F.R. and Wolfendale, A.W., editors, *Secular solar and geomagnetic variations in the last 10,000 years*, Dordrecht: Kluwer, 245–66.

—— 1989: Atmospheric ^{14}C and century-scale solar oscillations. *Nature* 338, 405–08.

—— 1993: Modeling atmospheric ^{14}C influences and radiocarbon ages of marine samples to 10,000 BC. *Radiocarbon* 35, 137–89.

Stuiver, M. and **Pearson, G.W.** 1992: Calibration of the radiocarbon time scale 2500–5000 BC. In Taylor, R.E., Long, A. and Kra, R.S., editors, *Radiocarbon after four decades: an interdisciplinary perspective*, New York: Springer-Verlag, 19–33.

—— 1993: High-precision bidecadal calibration of the radiocarbon time scale, AD 1950–500 BC and 2500–6000 BC. *Radiocarbon* 35, 1–23.

Stuiver, M. and **Polach, H.A.** 1977: Discussion: reporting of ^{14}C data. *Radiocarbon* 19, 355–63.

Stuiver, M. and **Quay, P.D.** 1980: Changes in atmospheric carbon-14 attributed to a variable sun. *Science* 207, 11–19.

—— 1981: Atmospheric ^{14}C changes resulting from fossil fuel CO_2 release and cosmic ray flux variability. *Earth and Planetary Science Letters* 53, 349–62.

Stuiver, M. and **Reimer. P.J.** 1993: Extended ^{14}C data base and revised CALIB 3.0 ^{14}C Age calibration program. *Radiocarbon* 35, 215–30.

Stuiver, M., Östlund, H.G. and **McConnaughey, T.A.** 1981: GEOSECS Atlantic and Pacific ^{14}C distribution. In Bolin, B. editor, *Carbon Cycle Modelling. SCOPE, 16*, New York: John Wiley, 201–21.

Stuiver, M., Braziunas, T.F., Becker, B. and **Kromer, B.** 1991: Climatic, solar, oceanic, and geomagnetic influences on late-glacial and Holocene atmospheric $^{14}C/^{12}C$ change. *Quaternary Research* 35, 1–24.

Talma, A.S. 1990: Radiocarbon age calibration of marine shells. *Quarterly Report, Quaternary Dating Research Unit*, CSIR, Pretoria, 10pp.

Taylor, K., Rose, M. and **Lamorey, G.** 1992: Relationship of solar activity and climatic oscillations on the Colorado plateau. *Journal of Geophysical Research* 97, 15803–11.

Taylor, K.C., Lamorey, G.W., Doyle, G.A., Alley, R.B., Grootes, P.M., Mayewski, P.A., White, J.W.C. and **Barlow, L.K.** 1993: The 'flickering switch' of late Pleistocene climate change. *Nature* 361, 432–36.

van Loon, H. and **Labitzke, K.** 1988: Association between the 11-year solar cycle, the QBO, and the atmosphere. Part II: Surface and

700 mb in the Northern Hemisphere in winter. *Journal of Climate* 1, 905–20.

Vautard, R. and **Ghil, M.** 1989: Singular spectrum analysis in nonlinear dynamics, with applications to paleoclimatic time series. *Physica* 35D, 395–424.

Weaver, A.J., Sarachik, E.S. and **Marotze, J.** 1991: Freshwater flux forcing of decadal and interdecadal oceanic variability. *Nature* 353, 836–38.

Wigley, T.M.L. and **Kelly, P.M.** 1990: Holocene climatic change, ^{14}C wiggles and variations in solar irradiance. *Philosophical Transactions of the Royal Society of London* A 330, 547–60.

Wilson, R.C. and **Hudson, H.S.** 1988: Solar luminosity variations in solar cycle 21. *Nature* 332, 810–12.